DISSERTATION

APPLICATION OF FORCE PREDICTION TO ROTATING EQUIPMENT USING PSEUDO-INVERSE TECHNIQUES

Submitted by

Mitchell Stansloski

Department of Mechanical Engineering

In partial fulfillment of the requirements

For the Degree of Doctor of Philosophy

Colorado State University

Fort Collins, Colorado

Spring 2010

COLORADO STATE UNIVERSITY

March 11, 2010

WE HEREBY RECOMMEND THAT THE DISSERTATION PREPARED UNDER OUR SUPERVISION BY MITCHELL STANSLOSKI ENTITLED APPLICATION OF FORCE PREDICTION TO ROTATING EQUIPMENT USING PSEUDO-INVERSE TECHNIQUES BE ACCEPTED AS FULFILLING IN PART REQUIREMENTS FOR THE DEGREE OF DOCTOR OF PHILOSOPHY.

Committee on Graduate Work

Paul Wilbur

Bryan Willson

Bogusz Bienkiewicz

Advisor: Fred W. Smith

Department Head: Allan Kirkpatrick

ABSTRACT OF DISSERTATION

APPLICATION OF FORCE PREDICTION TO ROTATING EQUIPMENT

USING PSEUDO-INVERSE TECHNIQUES

Extracting forcing functions for the purposes of signature analysis and load computation will improve root cause analysis on costly failures of rotating industrial equipment. By utilizing vibration signature response data and frequency response functions, both traditional troubleshooting technologies, the inverse method of force prediction has a high likelihood of becoming a useful force prediction tool to industrial maintenance staff. In prior research, force prediction using inverse methods has been studied and proven valid for a number of uni-axial structural configurations and external dynamic loadings. Minimal previously published studies have addressed computing internal forcing functions within rotating systems using these inverse techniques with experimental transfer functions. In this research, proof of concept is first obtained by applying the inverse method to a closed form solution of a rotating rigid shaft and disk assembly. Then, the method is validated with experimental data taken from a flexible rotating shaft system. Once validation is obtained, various rotating shaft speeds and loadings are studied. It is shown that this method can be an effective and accurate tool for root cause analysis in rotating industrial machinery.

Mitchell Stansloski, PE
Department of Mechanical Engineering
Colorado State University
Fort Collins, CO 80523
Spring 2010

Table of Contents

Table of Figures

Introduction

A major cost item in industry is the maintenance and repair of rotating industrial equipment such as pumps, compressors, manufacturing line components, etc. For a number of years, it has been standard practice to use vibration signatures as a way to predict the onset of mechanical problems before they cause a major failure and unplanned shutdown of production lines. Typical vibration signature analysis performed on industrial rotating equipment uses response spectral data. For this type of analysis, vibration transducers are mounted on the support system (e.g. bearing housings) as shown in Figure 1 and measure that system's response to forces as the machine is operating.

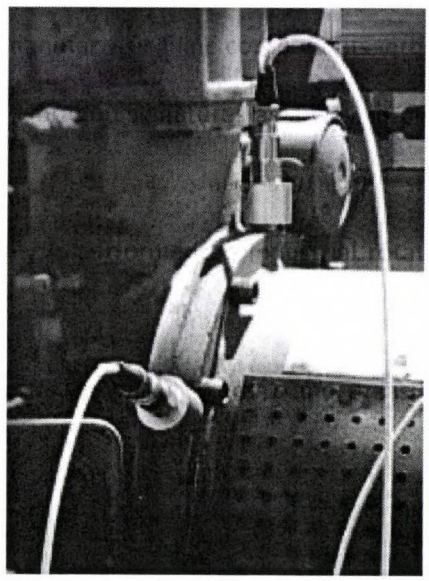

Figure 1 - Vibration Sensors Mounted on a Machine's Housing

Then it is typically found that the response signatures change with time. For example amplitudes might increase to excessive levels indicating a problem. Once such a condition is reached, attempts are then made to diagnose the cause of any problems that might be developing with the machine and undertake repairs before a problem becomes a major one. These diagnoses are based upon knowledge of the configuration details of the machine and the experience of the analysts rather than based upon a specific solution algorithm.

Also, response spectral data can hide the true root cause of the excessive vibration amplitudes. Aggravating conditions such as bearing clearances, beat frequencies, weak structural supports, and resonance can all dominate the response spectrum and mask the underlying force such as rotor unbalance or coupled shaft misalignment. Obtaining forcing functions, rather than response functions, would unveil the root cause problem, thereby removing the mask.

For example, Figure 2 gives a vibration response spectrum to an unbalance force aggravated by looseness.

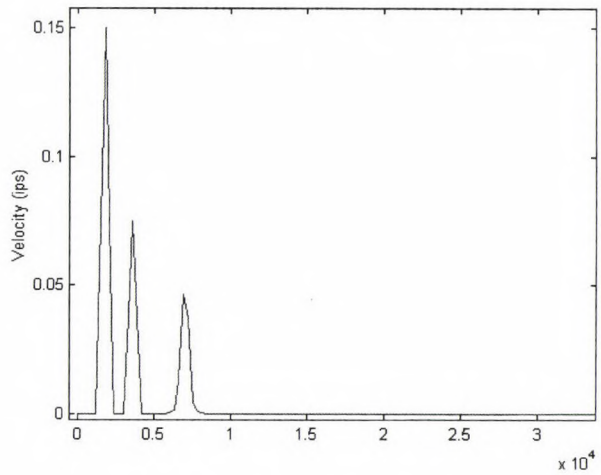

Figure 2 - Unbalance Aggravated by Looseness

In this graph, as is typical in industrial vibration signature analysis, the amplitude is measured in velocity in inches per second and frequency is measured in cycles per minute. In this case, a structural looseness has aggravated the response to the unbalance force resulting in harmonics of the unbalance frequency (in this case 1800 CPM) to be present. But an unbalance force is only applied at one frequency, and it is equal to the rotational speed of the rotating component.

Another example of aggravating conditions masking the true root source of the excessive vibration is illustrated in Figure 3.

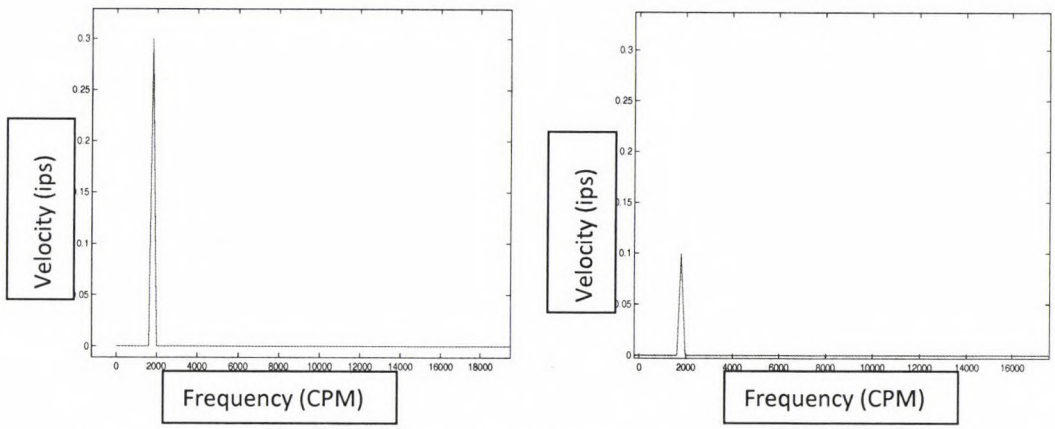

Figure 3 - Comparison of Horizontal and Vertical Plane Response to Unbalance Force

The vibration spectrum on the left shows the response to an unbalance force in the horizontal plane of this particular machine. The spectrum on the right shows the vibration response to the same unbalance force, but in the vertical plane. Note that the amplitude in the horizontal plane is three times larger than the amplitude in the vertical plane. The data of Figure 3 are representative of actual field situations experienced by the author. In this case the amplitude

difference was not caused by rotor unbalance but instead was caused by a structural resonance, a weakness, or a looseness that was aggravating the unbalance force in the horizontal plane resulting in inflated horizontal plane amplitude.

The vibration analyst knows that an unbalance force is equal in all planes though, and accordingly is likely to misdiagnose the true root cause of the excessive vibration as something other than unbalance because the two amplitudes are not equal. The result of this misdiagnosis is that work will be planned and production downtime scheduled in order to make a repair, but there will be no improvement of the vibration response once the repair is completed because, while the actual problem was unbalance, the unbalance was not repaired.

Having the ability to analyze forcing functions would be much more straight-forward than analyzing response functions since the influence of the aggravating conditions is removed when computing the predicted force. The vibratory response measured on a rotating system includes the effects of the forcing functions that the proposed method is intended to determine. The information needed to calculate and present them is routinely available and in fact, collected every day in traditional vibration condition monitoring programs. It just needs to be extracted from the data by stripping away the confusing effects of the aggravating conditions.

In summary, calculating loads from response vibration data has the potential to dramatically improve the accuracy of determining root cause sources. It can also quantify, and thereby, prioritize the repairs and improvements that need to be made. Lastly, it can be used in finite element loading simulations to aid in design.

Background

The idea for determining forces in a rotating system using inverse methods is the culmination of two different previous approaches for computing load. The notion of quantifying loads on a rotating shaft is inspired by the application of traditional forward methods using radio frequency strain gauges. The idea for using non-traditional inverse methods comes from recent research applied to structural vibrations(Hillary & Ewins, 1984).

Traditional methods of computing forces are based on forward methods. One simple example of a forward method on a static system is to compute the force exerted on a linear spring based upon measurement of the displacement. Let X be the measure of the displacement of the spring. Using Hooke's Law, the force can be directly computed by multiplying the spring constant, K, by the displacement of the compressed spring as shown in Equation 1.

$$F = KX \tag{1}$$

Another example of a traditional forward method, which is closer to the problem defined in this dissertation since it applies to a rotating shaft, is computing torque on the shaft from the shear stress. Shear stress is proportional to shear strain, which can be measured directly. Let γ be the shear strain, G be the shear modulus, J be the polar moment of inertia, c be the radius of the shaft, and τ be the shear stress.

Equation 2 gives the relationship between shear stress and strain.

$$\tau = G\gamma \tag{2}$$

Equation 3 gives the relationship between shear stress and torque. Rearranging Equation 3 to solve for torque and substituting Gγ for τ from Equation 2 into Equation 4 gives a forward method for computing torque based on measured shear strain.

$$\tau = \frac{Tc}{J} \tag{3}$$

$$T = \frac{G\gamma J}{c} \tag{4}$$

The shear strain is obtained by using a radio frequency strain gauge attached to shafts using adhesives. In this method shear strain is measured as the shaft rotates and is used in this forward manner to compute the applied torque. Determining dynamic load in this manner for rotating flexible systems is a problem that has been investigated thoroughly for decades. But because this method for quantifying loads is cumbersome and more readily applied in a research environment, it is not a common practice by maintenance and reliability personnel in an industrial setting. Also, it is limited because it can only measure torsion reactions in the shaft, and no reactions in the bearing. A more recent study using strain gauges to measure force was conducted at Texas A&M University (Zutavern & Childs, 2008). In this research, fiber-optic strain gauges were applied to magnetic bearings to determine the forces applied through them. But magnetic bearings are not yet common among industrial turbomachinery. So, the

industrial community needs a more effective way to quantify loads on a rotating shaft and its bearings.

In the late 1970's, force determination was first investigated from the reverse, or rather inverse, point of view (Bartlett & Flannelly, 1979). But it was only applied using uni-axial responses to the vibrating system within the supporting structure. Rather than use strain data gathered from strain gauges, researchers began using vibration acceleration or displacement response data gathered from transducers that were mounted on the structure in question.

The first step in the inverse method is to define a transfer function between a known force input, and a measured vibration response output. Figure 4 depicts the concept of this transfer function.

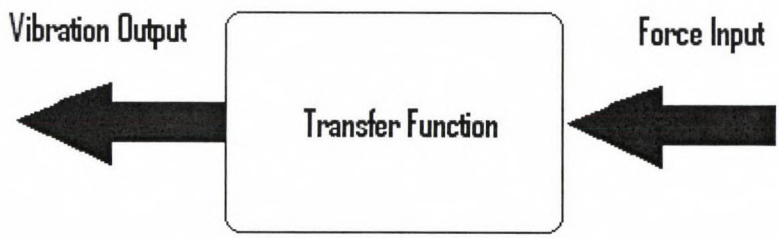

Figure 4 - Force Input and Vibration Response

The source for the force input can be one of several, with one criterion being that the source is able to excite a wide range of frequencies. One possible source of force input is a random frequency generator that is driving a portable shaker. The shaker is attached to a system by connecting a long slender rod, or "stinger" to it. Then a broadband random frequency signal is pulsed through the shaker. The shaker then excites the system with this known force input and

a vibration response to that known input is measured. Another option is to use a variable frequency generator as an input to a portable shaker. This device varies a signal from a minimum frequency to some pre-defined maximum limit. This variable frequency signal is used to generate vibration by the shaker and that vibration is applied to the system through the stinger. The vibration response to that known input force is then measured throughout the system in question.

All of the previous research (Bartlett & Flannelly, 1979)(Hillary & Ewins, 1984)(Fabunmi, 1986) using inverse methods and structural vibrations has imparted a force and measured its response using techniques as shown in Figure 5. In Figure 5, a shaker is used to impart a known artificial load along a single axis to a non-rotating system. The system in this case is a shaft supported by bearings mounted to a plate.

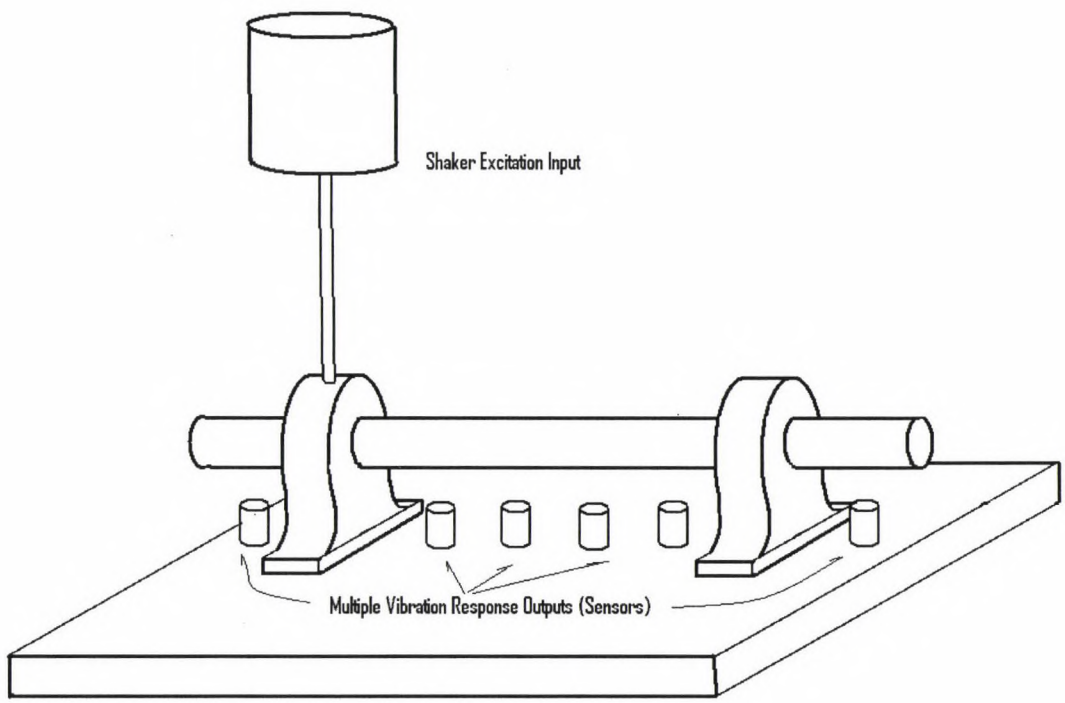

Figure 5 - Force Input and Vibration Output on Non-Rotating Shaft

The objective in the previous research was to characterize the forces as they were reacted to by the supporting structure, in this case the plate. Loads were delivered uni-axially and the reactions to those loads were measured uni-axially. They were not attempting to describe the forces within a rotating shaft.

Later research (Fabunmi, 1986) added measurement of multiple responses, like those shown in Figure 5. This was done in an effort to improve the accuracy of the forces predicted. Because there was participation of multiple modal frequencies in many of these cases, the principal of modal superposition and a least squares approximation of the multiple responses were applied in order to improve the predictability of the structural forces.

A new problem is introduced in this dissertation with the objective of computing forces within the rotating shaft. A rotating shaft has a gyroscopic effect which, among other factors, causes cross coupling between the reactions in two perpendicular planes. Since the cross-coupling is a function of the shaft's rotation, there are two requirements that must be met for an inverse method of force prediction to apply to this new problem. First, the shaft must be rotating while the force input is applied. Second, the force must be applied and the reactions measured in two perpendicular planes. Figure 6 illustrates this new problem.

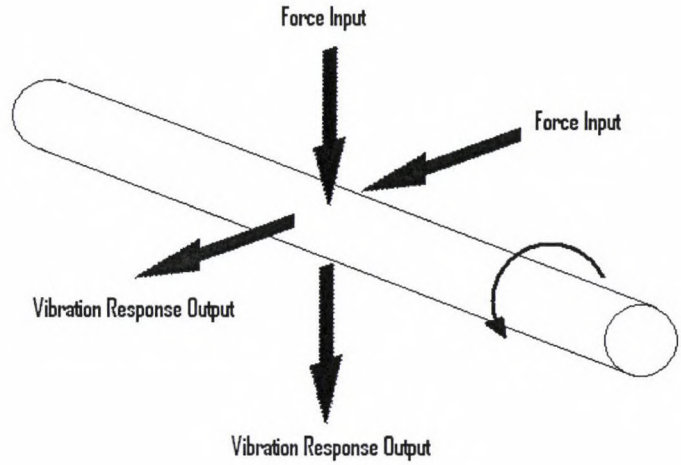

Figure 6 - Force Inputs and Vibration Responses Outputs from a Rotating Shaft

While the portable shaker method is fine for the structural systems researched earlier(Bartlett & Flannelly, 1979)(Fabunmi, 1986)(Hillary & Ewins, 1984), it is not a practical way to impart the force to a rotating shaft. Since it requires the attachment of a "stinger" to the system, it cannot transmit force very easily to a rotating shaft. An impulse function delivered by a modal hammer blow is a better choice for the force input in this case.

An impulse function, when applied to a system, generates a broadband frequency energy input. In general, the shorter the duration of the impulse function, the higher the frequency range that is excited. An impulse is typically applied with a modal hammer with interchangeable tips. Each tip has varying hardness, which is designed to vary the duration of the impulse, thereby varying the excitation frequency range. A modal hammer is essentially a calibrated dynamic force transducer. Since the hammer does not have to be permanently attached to the shaft the way a shaker does in order to impart its force, it is a better choice for the rotating shaft.

One possible source of error that is introduced by using a modal hammer to apply an impulse function to a rotating shaft is skidding that may occur during the short duration that the tip is in contact with the spinning shaft. This would not affect the signal measured by the dynamic force transducer embedded in the tip of the hammer since it is a unidirectional sensor with transverse sensitivity of less than 1%. But it may cause error by introducing a slight lateral component of the force input to the system rather than a purely radial input. Testing this source of error is discussed further in the "Recommendations for Future Research" section of this dissertation. Figure 7 illustrates the experimental setup for the research undertaken in this dissertation.

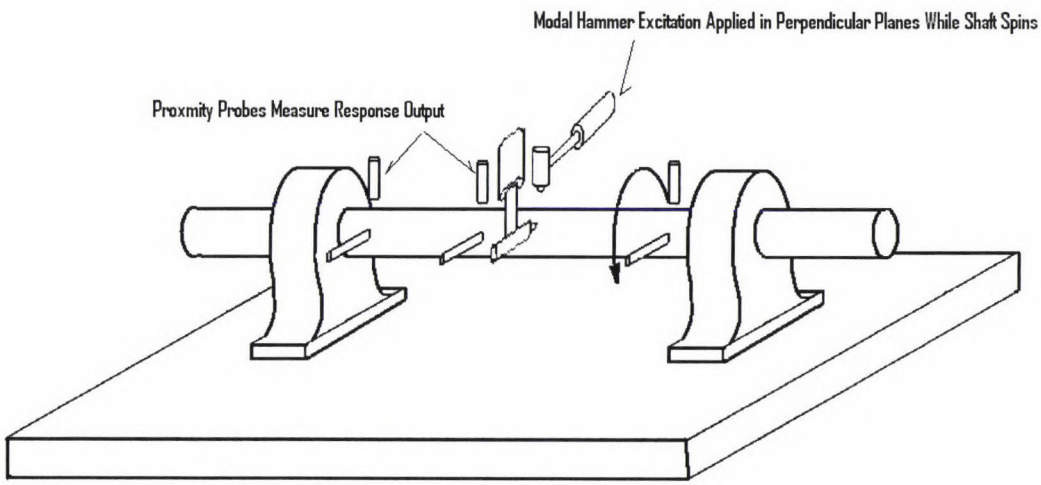

Figure 7 - Impulses Applied to a Rotating Shaft in Perpendicular Planes

In the figure, a modal hammer is used to apply an impulse in two perpendicular planes while the shaft is spinning. Proximity probes are used to measure the displacement response of the shaft.

So far the differences between the previous research and this study include applying a modal hammer blow to a rotating shaft in perpendicular planes while also measuring responses in

perpendicular planes. As mentioned, this is required since the objective is to compute forces within the rotating shaft and the reactions necessary to compute those forces are cross-coupled as well as directly affected by the speed at which the shaft rotates. Another difference that should be noted between the previous research and this study is the number of responses measured. Since the previous work was predicting forces uni-axially along the length of some structure, including many responses was advantageous so that the accuracy could be improved by applying the aforementioned modal superposition principal as well as a least squares approximation for the solution (Fabunmi, 1986). In this case, however, the objective is to quantify the loads within a rotating shaft. So if more reaction locations were required, they would be added circumferentially around the periphery of the shaft rather than along its length. But since the mode shapes of a spinning shaft are symmetrical about its axis, the principal of modal superposition does not apply and only two perpendicular reactions are required. Additional reactions measured circumferentially would not improve the accuracy for this problem as they did when measured uni-axially in different locations along a structure for the problems previously researched (Fabunmi, 1986).

Multiple locations for vibration response measurement were used in this research in order to determine how the force prediction accuracy would change as a function of response location relative to the supporting bearings as well as the anti-node position of shaft deflection.

For simplicity's sake, throughout this dissertation the previous research will be referred to as that applied to structural vibration, and this research will be referred to as that applied to a rotating shaft.

The general procedure for extracting loads from response data follows. In this case A(ω) is the Fourier transform of the vibration output response, F(ω) is the Fourier transform of the forcing function input, and H(ω) is the transfer function.

A known impulse force, F(t) is applied to a system using the modal hammer. Then the output vibration response, A(t), is measured. The force input signal, F(t), and vibration output, A(t), are converted to the frequency domain using the Fourier transform to obtain F(ω) and A(ω) respectively. The transfer function, computed in the frequency domain, is defined in Equation 5.

$$\boldsymbol{H(\omega) = \frac{A(\omega)}{F(\omega)}} \tag{5}$$

Subsequently, a new unknown force, $F_1(t)$ is applied and a new vibration response is measured, $A_1(t)$. Pre-multiplying the Fourier transform of $A_1(t)$ by the inverse of the original transfer function returns the unknown forcing function $F_1(\omega)$, as shown in Equation 6.

$$\boldsymbol{F_1(\omega) = H(\omega)^{-1} A_1(\omega)} \tag{6}$$

This is the essence of the inverse force prediction method. F_1 is a representation of the force being sought by determination of the transfer function and then measurement of the vibration response in a rotating system. $H(\omega)^{-1}$ in Equation 6 is the traditional inverse, and that inverse to the transfer function matrix exists if the matrix is square and has full rank (Strang, 1988). When the inverse fails to exist, a natural substitute is called the pseudo-inverse (Strang, 1988). There may be cases in the application of inverse force prediction methods when the transfer function

matrix is not invertible, such as when it is either rank deficient, or ill conditioned respectively. In these cases, the pseudo-inverse procedure provides a suitable way to calculate the inverse. Furthermore, in the case where the matrix is invertible or difficult to invert with straight-forward methods, the traditional inverse and pseudo-inverse are the same (Strang, 1988). Therefore, the pseudo-inverse function will work in more applications than the traditional inverse function. For this reason, inverse force prediction should utilize the pseudo-inverse method in practical application. Matlab's pseudo-inverse, or "pinv", function is used for computations in this dissertation. The pseudo-inverse function can be computed using singular value decomposition and is more fully described in the analysis section of this dissertation.

Applications found in the literature review have applied inverse force determinations to structural vibration systems. External periodic forces have been successfully computed on these systems. Beams have been modeled and simulated loads applied (Hillary & Ewins, 1984). Bartlett and Flannelly applied shaker testing at a simulated rotor hub in order to characterize the forces distributed throughout the simulated helicopter fuselage (Bartlett & Flannelly, 1979). A group from Chuo University in Tokyo, Japan considered some practical cases(Okubo, Tanabe, & Tatsuno, 1985). They estimated forces from an engine to its mounts, an air conditioner to its piping, and a machine tool to its work piece using the pseudo-inverse method. In follow up to the work at Chuo University, forces delivered to an automobile frame from the engine were estimated (Matsumura, 1985). Further research at Chuo University includes prediction of transmitted forces between components for the purpose of noise reduction (Toi, Aoyama, & Okubo, 1995), and the prediction of forces in an automobile engine in a high frequency range (Okubo, Shimamura, & Toi, 2006). A project at the Huazhong University in China estimated forces excited by machinery vibration in a ship (Yuan, Zhu, Zhang, & Zhang, 2007). A group from

the Darmstadt University of Technology in Germany used an inverse method of force prediction to determine rotor imbalance distributions(Peters, Nordmann, Domes, & Maass, 2004). This group solved a forward problem first by creating an extensive finite element model in order to predict the vibratory response to a proposed imbalance. Then they used that model, combined with dynamic measurements in an inverse manner, to determine the rotor imbalance distributions. Another study that used finite elements to predict vibratory sources was one conducted in France (Chiementin, Bolaers, Rasolofondraibe, & Dron, 2008). This group created a finite element model of a test fixture to generate the modal matrices used for the inverse force prediction. They then applied numerical simulated sources as well as experimental sources, and predicted those sources using the finite element derived matrices. Not only is using the finite element derived matrices more complicated and thereby more costly than the experimental methods used in this dissertation, it is also subject to more uncertainty due to difficult to define boundary conditions. Studies have also been done to estimate the shock loads on computer cabinets when dropped (Avitabile & Piergentili, 1999). These structural vibration systems, such as the engine mounts, air conditioner piping, and machine tool work piece, have been well researched and the results documented. For example, Ewins even describes force determination from structural vibration response in his book, "Modal Testing" (Ewins, 2000).

In addition to the variety of structural vibration applications studied, the methods for extraction themselves have also been the subject of scrutiny. Papers by Fabunmi, and by Desanghere and Snoeys discuss the conditions and applications when inverse method force determination will be accurate (Fabunmi, 1986)(Desanghere & Snoeys, 1985). A study done at the Imperial College of Science and Technology compared the results of force prediction using accelerometers and

strain gauges (Hillary & Ewins, 1984). A comparison was also made between time domain and frequency domain force prediction methods (Dos Santos & Varoto, 1998).

The literature review reveals that minimal research has been done on systems with the objective of characterizing the forces within a rotating shaft. Perhaps this is because a rotating system has additional hurdles that are not present in the previous studies. The transfer functions measured in these uni-axial structural vibration systems are markedly different than the transfer functions that characterize a rotating shaft. A uni-axial structural system's modal matrices are symmetric, allowing for reciprocity to apply, which gives straight-forward matrix inversion solutions. A rotating system's modal matrices are not symmetric due to a number of factors. First, gyroscopic effects, caused by lateral vibration on a rotating shaft, will add skew symmetric terms to the velocity matrix. Additional modes are added as a result of this skew symmetry. The gyroscopic effects also make the principal frequencies dependent on the operating speed of the rotor. Also, internal damping and hydrodynamic bearing behavior can add skew symmetric terms to the stiffness matrix. It would not be applicable to collect a structural-based transfer function and apply it to a rotating member. Merely collecting a transfer function on a rotating member presents some additional challenges (Ewins, 2000), which are discussed in the experimental section of this dissertation.

Inverse methods for force prediction as applied to reactions of a rotating shaft are more viable than the traditional forward methods because the industrial community will more readily accept load quantification in this manner for several reasons. First, traditional forward methods of determining actual loads are cumbersome and therefore impractical in many applications. Secondly, many industrial maintenance personnel already collect vibration response data on a

regular basis. Third, many of them are also familiar with impulse testing using a modal hammer to determine natural frequencies. Computing a response function from those impulse tests would not be an intimidating step-up in technology so that this new procedure is likely to be useful, accepted and used in industry.

Theoretical Approach

A partial proof of concept for this inverse method of force prediction is obtained by performing a closed form solution on a relatively simple rotating system and then demonstrating that the pseudo-inverse method applied to simulated vibration response data will return the correct forces when applied to the system. The results of the closed form solution are presented in the following. The model will be a rigid shaft of length L, with a rigid disk attached to it. The disk is mounted on the free end of the shaft, and the other end of the shaft is pinned. This model is shown in Figure 8. The free end of the shaft is supported with a flexible bearing, which has vertical and horizontal stiffness variables k_y and k_x respectively. The polar mass moment of inertia of the disk and shaft is J, and the mass moment of inertia about the lateral axis is I_0. The rotor has an angular velocity Ω_z.

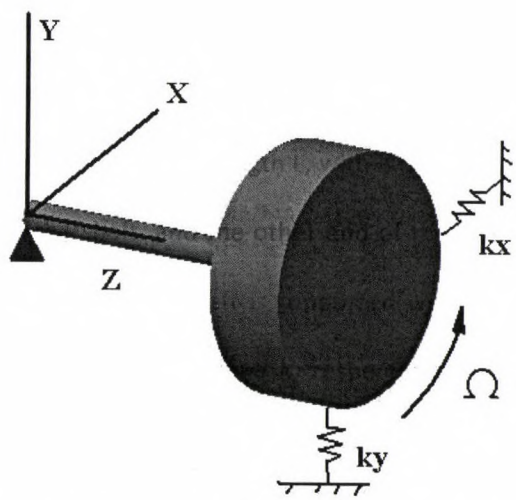

Figure 8 - Theoretical Model of Spinning Disk

Damping is neglected in the closed form solution since damping factors for industrial pumps and fans vary from 1 – 5%, with factors as high as 10% considered atypical. A numerical experiment was conducted to gather data for the input to the pseudo-inverse method.

The solution begins by writing the equations of motion for the system. Next the modal matrices are computed, and the transfer function matrix is assembled for a force input. Then, an unbalance forcing function is applied, and its response computed. That response is then pre-multiplied by the inverse of the transfer function to determine if the correct unbalance force can be calculated. In addition, the transfer function matrix condition number is computed and plotted versus frequency.

Given a transfer function matrix, H, the condition number is defined in Equation 7 (Strang, 1988) and is a ratio of the largest singular value of H to the smallest singular value.

$$\boldsymbol{Cond(H)} = \|\boldsymbol{H}\|\left\|\boldsymbol{H^{-1}}\right\| \tag{7}$$

where $\|H\|$ is the 2-Norm of the transfer function matrix H. The norm of matrix measures the largest amount by which any vector is amplified by matrix multiplication (Strang, 1988). The 2-Norm, also known as the Euclidean Norm, is defined as the largest singular value of a matrix and is defined in Equation 7a.

$$\|H\| = \sqrt{\lambda_{max}(H^T H)} \tag{7a}$$

In general terms, the condition number is a measure of the sensitivity of a matrix to error in numerical operations such as matrix inversion. In terms of force prediction, the condition

number is a measure of the sensitivity of the calculation of the predicted force to errors in the inversion of the transfer function matrix. When the condition number is large, small changes in the transfer function, H, can lead to large errors in the predicted force (Varoto, 1996) (Stevens, 1987).

Starting with the equations of motion:

$$\frac{I}{L}\ddot{x} + \frac{J\Omega}{L}\dot{y} + k_x L x = 0 \tag{8}$$

$$\frac{I}{L}\ddot{y} - \frac{J\Omega}{L}\dot{x} + k_y L y = 0 \tag{9}$$

where I is the mass moment of inertia about the x and y axes, L is the shaft length, J is the polar mass moment of inertia, k_x is the stiffness coefficient along the X axis, k_y is the stiffness coefficient along the Y axis, Ω is the shaft turning speed, x and its derivatives define motion along the X axis, and y and its derivatives define motion along the Y axis.

Since typical shaft vibration amplitudes are less than 0.005 inches in industrial machinery, small displacements are assumed here.

Note the presence of the Coriolis Acceleration terms ($\Omega\dot{y}$ and $\Omega\dot{x}$) resulting from lateral vibration of a rotating shaft. These terms couple the two equations, and generate a velocity coefficient matrix even though there is no damping considered (Ewins, 2000). The effect of this coupling is that, even with symmetric bearing stiffness, two principal frequencies are present. This is not the case for a structural system.

To solve the differential equations of motion, the first step is to assume a solution for the responses along the x-axis and y-axis, namely x and y respectively.

Assume y is of the form found in Equation 10 and x is of the form in Equation 11.

$$y = Ye^{i\omega t} \tag{10}$$

$$x = Xe^{i\omega t} \tag{11}$$

Differentiating for the velocities is shown in Equation 12 and Equation 13.

$$\dot{y} = i\omega Ye^{i\omega t} \tag{12}$$

$$\dot{x} = i\omega Xe^{i\omega t} \tag{13}$$

Differentiating again for the accelerations is shown in Equation 14 and Equation 15.

$$\ddot{y} = i^2\omega^2 Ye^{i\omega t} = -\omega^2 Ye^{i\omega t} \tag{14}$$

$$\ddot{x} = i^2\omega^2 Xe^{i\omega t} = -\omega^2 Xe^{i\omega t} \tag{15}$$

Substituting Equations 10, 11, 12, 13, 14, and 15 into Equations 8 and 9 gives Equation 16 and Equation 17.

$$\frac{I}{L}\left(-\omega^2 Xe^{i\omega t}\right) + \frac{J\Omega}{L}(i\omega Ye^{i\omega t}) + k_x LXe^{i\omega t} = 0 \tag{16}$$

$$\frac{I}{L}\left(-\omega^2 Y e^{i\omega t}\right) - \frac{J\Omega}{L}\left(i\omega X e^{i\omega t}\right) + k_y L Y e^{i\omega t} = 0 \tag{17}$$

Simplifying gives Equation 18 and Equation 19.

$$\frac{I}{L}(-\omega^2 X) + \frac{J\Omega}{L}(i\omega Y) + k_x L X = 0 \tag{18}$$

$$\frac{I}{L}(-\omega^2 Y) - \frac{J\Omega}{L}(i\omega X) + k_y L Y = 0 \tag{19}$$

Combining terms results in Equation 20 and Equation 21.

$$\left(k_x L - \frac{I}{L}\omega^2\right) X + \left(\frac{J\Omega}{L} i\omega\right) Y = 0 \tag{20}$$

$$\left(-\frac{J\Omega}{L} i\omega\right) X + \left(k_y L - \frac{I}{L}\omega^2\right) Y = 0 \tag{21}$$

Equation 20 and Equation 21 written in matrix form is shown in Equation 22. The skew symmetry resulting from the Coriolis Accelerations can be seen.

$$\begin{bmatrix} \left(k_x L - \frac{I}{L}\omega^2\right) & \left(\frac{J\Omega}{L} i\omega\right) \\ \left(-\frac{J\Omega}{L} i\omega\right) & \left(k_y L - \frac{I}{L}\omega^2\right) \end{bmatrix} \begin{pmatrix} X \\ Y \end{pmatrix} = 0 \tag{22}$$

For the non-trivial solution, the determinant of the matrix is set to zero in Equation 23.

$$det \begin{vmatrix} \left(k_x L - \frac{I}{L}\omega^2\right) & \left(\frac{J\Omega}{L} i\omega\right) \\ \left(-\frac{J\Omega}{L} i\omega\right) & \left(k_y L - \frac{I}{L}\omega^2\right) \end{vmatrix} = 0 \tag{23}$$

Computing the determinant is shown in Equation 24.

$$\left(k_x L - \frac{I}{L}\omega^2\right)\left(k_y L - \frac{I}{L}\omega^2\right) - \left(-\frac{J\Omega}{L}i\omega\right)\left(\frac{J\Omega}{L}i\omega\right) = 0 \tag{24}$$

This leads to the characteristic equation, which can be solved for the two principal frequencies, ω_1 and ω_2.

$$\frac{I^2\omega^4}{L^2} - \left[\frac{J^2\Omega^2}{L^2} + (k_x + k_y)I\right]\omega^2 + k_x k_y L^2 = 0 \tag{25}$$

By defining λ in Equation 26 and substituting it into Equation 25 gives Equation 27.

$$\lambda = \omega^2 \tag{26}$$

$$\frac{I^2\lambda^2}{L^2} - \left[\frac{J^2\Omega^2}{L^2} + (k_x + k_y)I\right]\lambda + k_x k_y L^2 = 0 \tag{27}$$

Equation 27 is of the standard form for use with the quadratic equation and can be solved for λ_1 and λ_2. This is shown in Equation 28 and Equation 29. Equation 26 is then used to compute ω_1 and ω_2.

$$\lambda_1 = \frac{\left[\frac{J^2\Omega^2}{L^2} + (k_x + k_y)I\right] - \sqrt{\left[\frac{J^2\Omega^2}{L^2} + (k_x + k_y)I\right]^2 - 4\frac{I^2 k_x k_y L^2}{L^2}}}{2\frac{I^2}{L^2}} \tag{28}$$

$$\lambda_2 = \frac{\left[\frac{J^2\Omega^2}{L^2}+(k_x+k_y)I\right]+\sqrt{\left[\frac{J^2\Omega^2}{L^2}+(k_x+k_y)I\right]^2-4\frac{I^2k_xk_yL^2}{L^2}}}{2\frac{I^2}{L^2}} \tag{29}$$

Next, the transfer function is computed. It is assumed that the general form of a force input is as shown in Equation 30.

$$F(t) = e^{i\omega t} \tag{30}$$

A transfer function can be defined, H(ω), that characterizes the relationship between the force input, and the vibration response output (Rao, 1986). This is presented in Equation 31 and Equation 32 where x(t) and y(t) are vibration responses along the x and y axes.

$$y(t) = H(\omega)\, e^{i\omega t} \tag{31}$$

$$x(t) = H(\omega)\, e^{i\omega t} \tag{32}$$

Applying the generalized force from Equation 30 to the equations of motion written in Equation 8 and Equation 9, gives Equation 33 and Equation 34.

$$\frac{I}{L}\ddot{\boldsymbol{x}} + \frac{J\Omega}{L}\dot{\boldsymbol{y}} + \boldsymbol{k_xLx} = \boldsymbol{e^{i\omega t}} \tag{33}$$

$$\frac{I}{L}\ddot{\boldsymbol{y}} - \frac{J\Omega}{L}\dot{\boldsymbol{x}} + \boldsymbol{k_yLy} = \boldsymbol{e^{i\omega t}} \tag{34}$$

The derivatives for velocity and acceleration are computed using Equations 31 and 32. Substituting the displacement, velocity, and acceleration terms into Equations 33 and 34 gives Equations 35 and 36.

$$\left(k_x L - \frac{I}{L}\omega^2\right) H(\omega) + \left(\frac{J\Omega}{L} i\omega\right) H(\omega) = 1 \tag{35}$$

$$\left(-\frac{J\Omega}{L} i\omega\right) H(\omega) + \left(k_y L - \frac{I}{L}\omega^2\right) H(\omega) = 1 \tag{36}$$

The matrix form of Equations 35 and 36 is shown in Equation 37.

$$\begin{bmatrix} \left(k_x L - \frac{I}{L}\omega^2\right) & \left(\frac{J\Omega}{L} i\omega\right) \\ \left(-\frac{J\Omega}{L} i\omega\right) & \left(k_y L - \frac{I}{L}\omega^2\right) \end{bmatrix} H(\omega) = 1 \tag{37}$$

Inverting the coefficient matrix gives the transfer function H(ω) in Equation 38.

$$H(\omega) = \begin{bmatrix} \left(k_x L - \frac{I}{L}\omega^2\right) & \left(\frac{J\Omega}{L} i\omega\right) \\ \left(-\frac{J\Omega}{L} i\omega\right) & \left(k_y L - \frac{I}{L}\omega^2\right) \end{bmatrix}^{-1} \tag{38}$$

The inversion is computed in Equation 39.

$$H(\omega) = \frac{1}{\frac{I^2\omega^4}{L^2} - \left[\frac{J^2\Omega^2}{L^2} + (k_x + k_y) I\right]\omega^2 + k_x k_y L^2} \begin{bmatrix} \left(k_y L - \frac{I}{L}\omega^2\right) & \left(-\frac{J\Omega}{L} i\omega\right) \\ \left(\frac{J\Omega}{L} i\omega\right) & \left(k_x L - \frac{I}{L}\omega^2\right) \end{bmatrix} \tag{39}$$

The general form of the transfer function matrix is presented in Equation 40.

$$H(\omega) = \begin{bmatrix} H_{yy}(\omega) & H_{yx}(\omega) \\ H_{xy}(\omega) & H_{xx}(\omega) \end{bmatrix} \tag{40}$$

Symmetric stiffness is assumed in Equation 41.

$$k_x = k_y \tag{41}$$

Using the general form of the transfer function matrix in Equation 40, and the calculated transfer function from Equation 39, gives the specific transfer functions in Equations 42 and 43.

$$H_{xx}(\omega) = H_{yy}(\omega) = \frac{\left(k_x L - \frac{I}{L}\omega^2\right)}{\frac{I^2\omega^4}{L^2} - \left[\frac{J^2\Omega^2}{L^2} + (k_x + k_y)I\right]\omega^2 + k_x k_y L^2} \tag{42}$$

$$H_{xy}(\omega) = -H_{yx}(\omega) = \frac{\left(\frac{J\Omega}{L}i\omega\right)}{\frac{I^2\omega^4}{L^2} - \left[\frac{J^2\Omega^2}{L^2} + (k_x + k_y)I\right]\omega^2 + k_x k_y L^2} \tag{43}$$

$H_{xx}(\omega)$ is the transfer function for a force applied along the x-axis and a vibration response measured along the x-axis. $H_{yy}(\omega)$ is the transfer function for a force applied along the y-axis and a vibration response measured along the y-axis. $H_{xy}(\omega)$ is the transfer function for a force applied along the x-axis and a vibration response measured along the y-axis. $H_{yx}(\omega)$ is the transfer function for a force applied along the y-axis and a vibration response measured along the x-axis.

Then, the following values were arbitrarily assigned in order to test the closed form solution. A Matlab program was written to perform the computations and is included in Appendix A.

$J = 6.452(10)^{-4}$ kg-m^2

$I = 8.39(10)^{-3}$ kg-m^2

$L = 0.09525$ m

$k_x = k_y = 350{,}000$ N/m

$\Omega = 188$ rad/sec

$0 < \omega < 1000$ rad/sec

$F_x = 10\cos(188t)$

$F_y = 10\sin(188t)$

The forces F_x and F_y represent the internal unbalance forces along the X and Y axes. Using Matlab to assemble the matrices and perform the computations, the following results were obtained:

The transfer functions H_{xx}, H_{yy}, H_{xy}, and H_{yx} are presented in Figure 9, Figure 10, and Figure 11. They are then assembled within the Matlab program to produce the transfer function matrix. The two principal frequencies are 608 rad/sec and 622 rad/sec respectively.

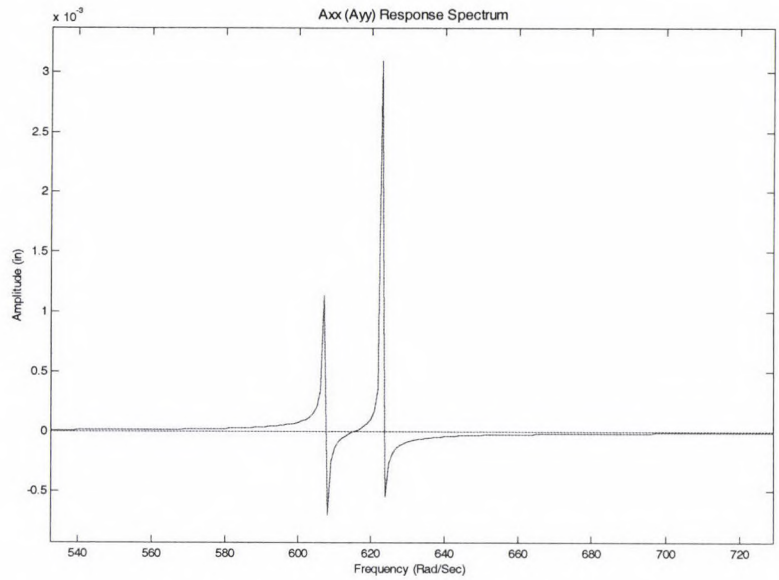

Figure 9 - Hxx Transfer Function

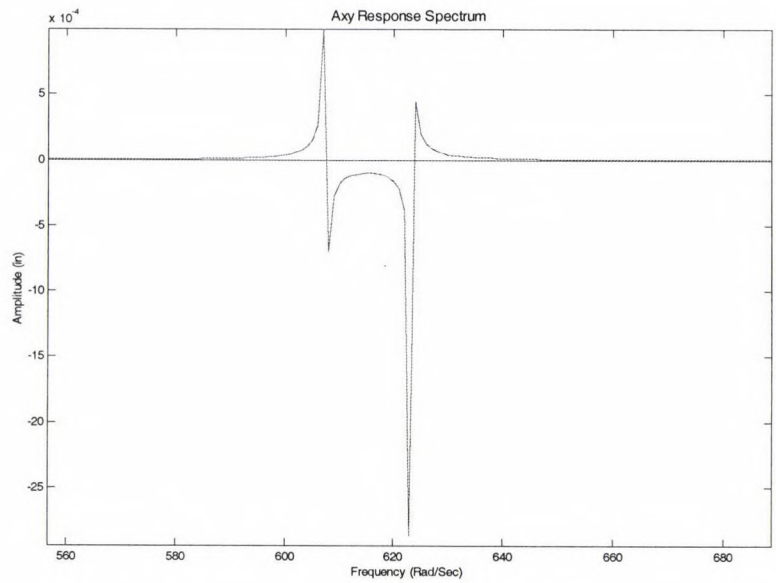

Figure 10 - Hxy Transfer Function

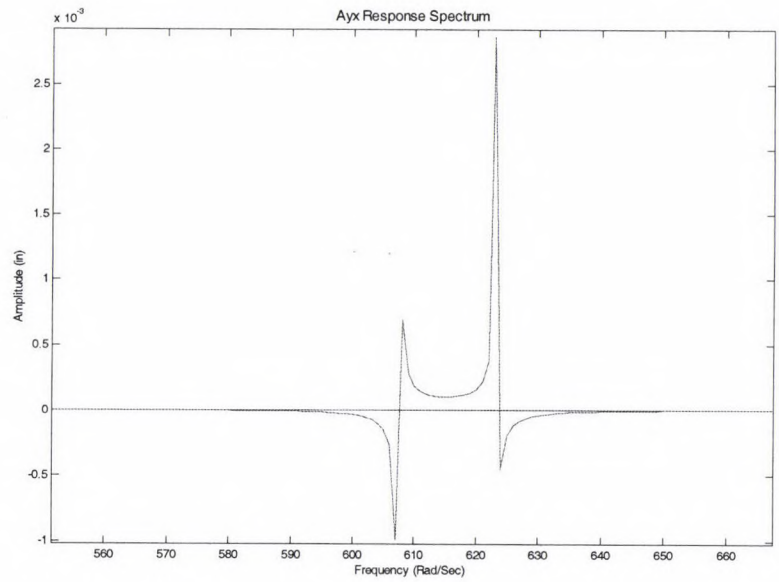

Figure 11 - Hyx Transfer Function

Figure 12 illustrates the actual applied force in the x-direction as it was defined at the start of this solution. The applied force in the y-direction is identical.

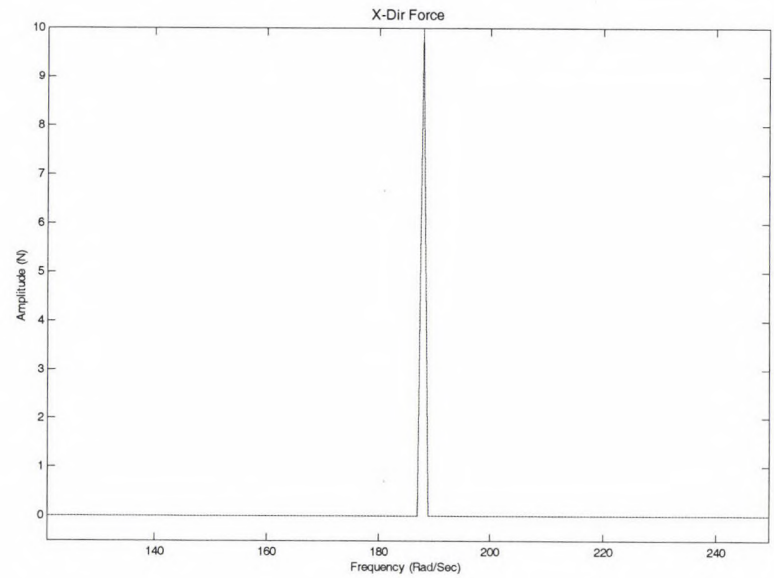

Figure 12 – Applied Force in X Direction

In Figure 13, the response to the unbalance is presented in the x-direction. The y-direction response is identical.

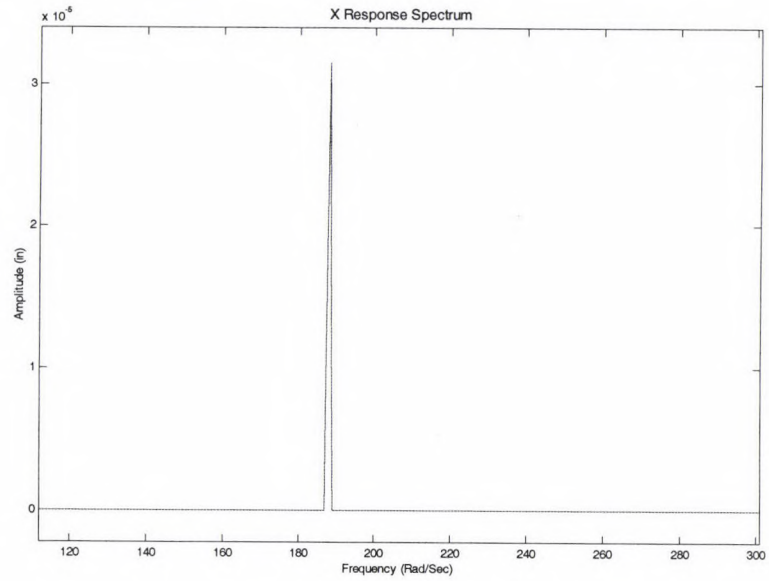

Figure 13 – X Direction Vibration Response to Force

Now, to demonstrate how the pseudo-inverse method is intended to work, the information in Figure 13 is taken to be input data within the Matlab program included in Appendix A. After pre-multiplying the x and y response data by the pseudo-inverse of the transfer function, the input force is predicted and presented in Figure 14. The predicted force exactly matches the original applied force as presented in Figure 12 thus demonstrating that the method works as expected and in this case provides the correct predicted forces based on displacement data (which would be measured in an industrial setting) as input.

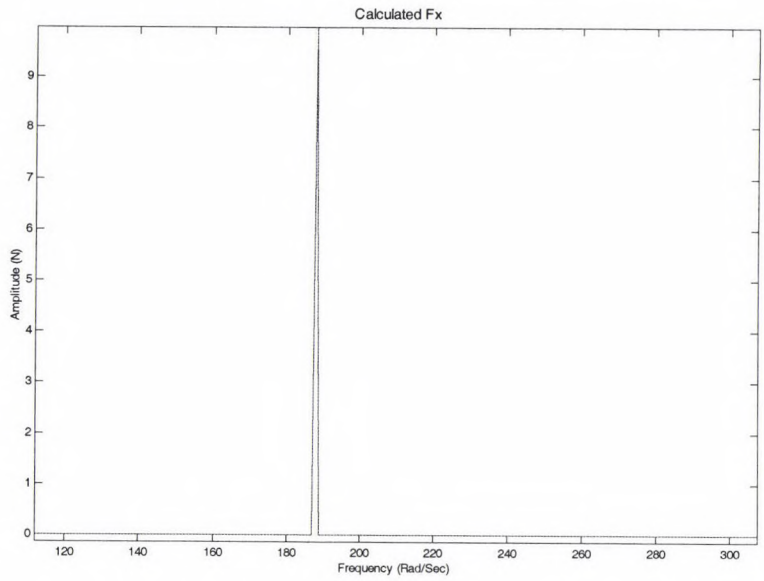

Figure 14 - Predicted Force in X Direction

Reviewing the transfer function matrix condition number, shown in Figure 15, reveals that there is no ill conditioning at the frequency being evaluated (Ω=188 rad/sec).

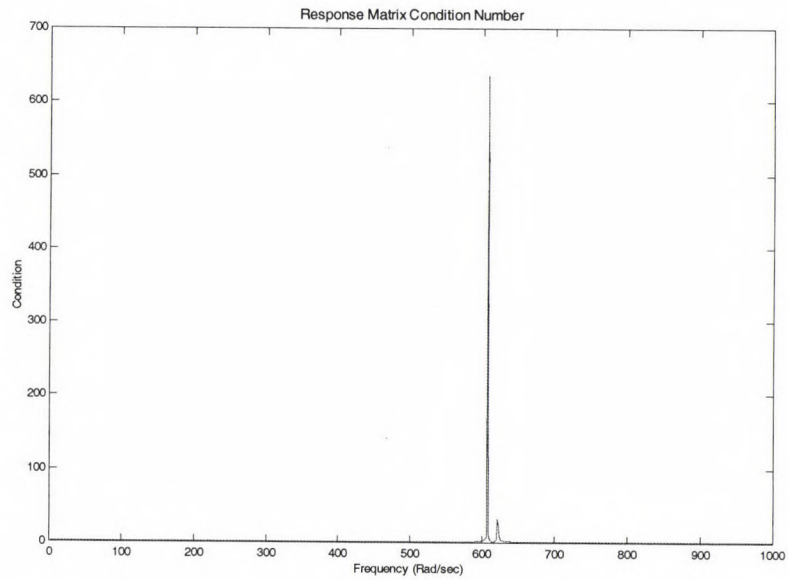

Figure 15 – Transfer Function Matrix Condition Number

Note that this is not the case at the principal frequencies. This is important because it suggests that force prediction using pseudo-inverse methods applied at a system's principal frequencies may not be accurate.

In order to determine if force prediction applied at a principal frequency is possible, at least in a closed form solution, the forcing frequency is changed to match a principal frequency. So, the applied forcing frequency (Ω = 640 rad/sec) was changed so that it would match the forward-precession principal frequency (the new ω_2 = 640 rad/sec, and ω_1 = 591 rad/sec), exciting a resonant situation. Figure 16 and Figure 17 show the transfer functions. Since the H_{yx} function is again skew symmetric to H_{xy}, it is not presented for brevity.

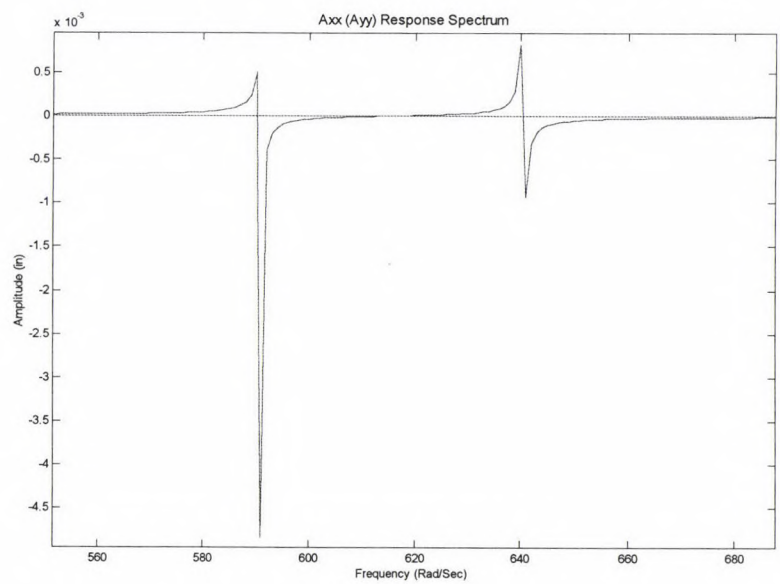

Figure 16 - Hxx Transfer Function

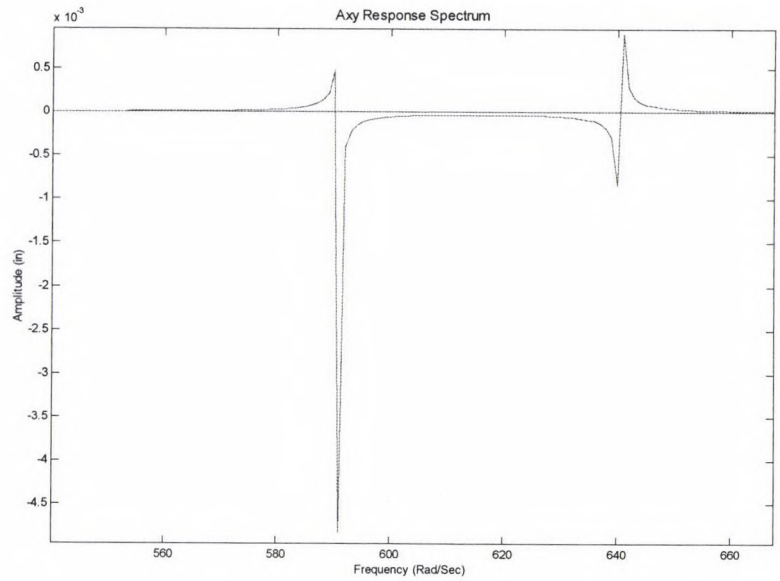

Figure 17 - Hxy Transfer Function

Figure 18 shows the response to the unbalance force in the x-direction. The identical y-direction response is not shown. Note that the amplitude has significantly increased due to the resonant condition. This is significant because resonance is one of several aggravating conditions that can mask the true root source of an excessive vibration. It does this by amplifying the response to the force in ways not indicative of the force it is aggravating. It does so in this case, yet the force prediction method still reveals the proper amplitude of the offending force in this closed form solution.

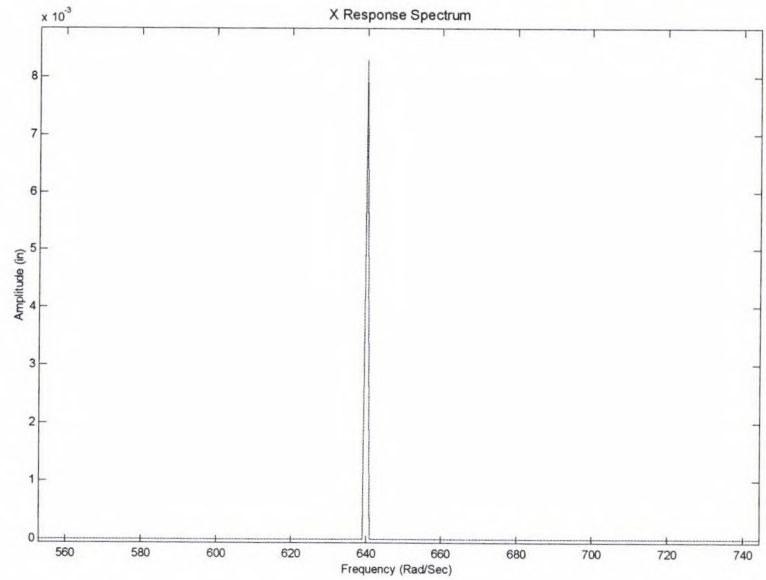

Figure 18 – X Direction Vibration Response to Force

Using the same calculation procedure as before, the predicted force is extracted and presented in Figure 19. Again, the predicted force matches the original applied force exactly.

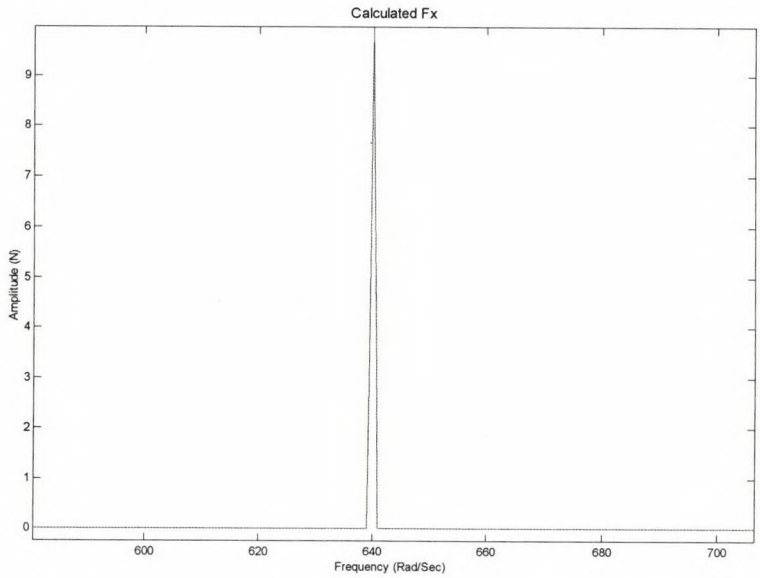

Figure 19 – Predicted Force in X Direction

However, the condition number shown in Figure 20 illustrates that the transfer function matrix is ill conditioned (high values) at both principal frequencies. It is ill conditioned because of the massive amplification of vibration response at resonance to a small input force. Due to this ill-conditioning, it is unlikely that this type of accuracy can be expected when computing forces at resonance in practical application. This fact will result in the elimination of this scenario in the development of the criteria for acceptability for the application of the pseudo-inverse method of force prediction.

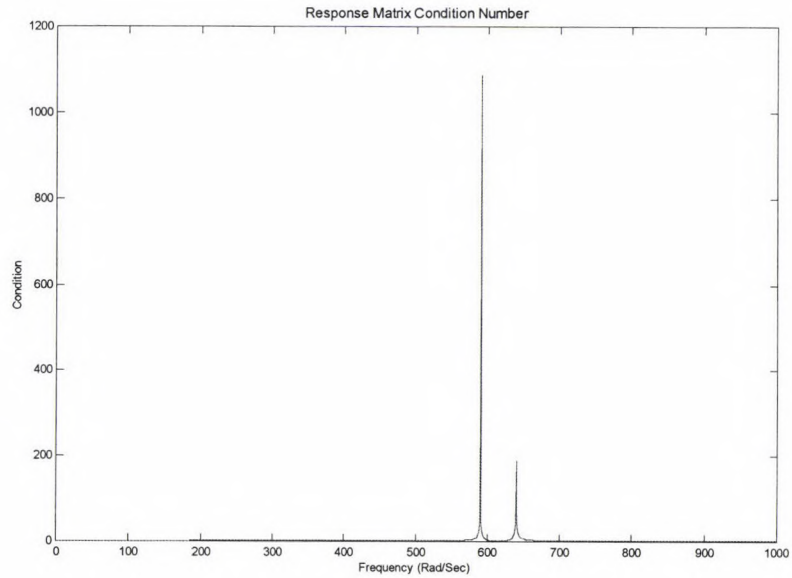

Figure 20 - Response Matrix Condition Number

The proof of concept is complete with the conclusion of this closed form solution. The predicted forces were 100% accurate as expected in both amplitude and frequency, however, in real world applications, there are issues that are not present in this closed form solution. Issues such as signal noise, averaging, and the physical application of an impulse to a spinning shaft will all affect the results in an industrial application.

So, in the next section of this dissertation, the pseudo-inverse analysis procedure is applied to an actual test rotor that, though more complex than the rotor modeled in the closed form solution and closer to a real world scenario, is still relatively simple.

Experimental Approach

The general procedure for the experimental approach included selecting a simple rotor and minimizing any forces, such as unbalance and shaft misalignment, that could cause the rotor to give a vibratory response. Then two known force inputs were applied as impulse functions in perpendicular planes while the rotor was operating. They had to be applied while the rotor was spinning because the response functions are dependent on operating speed. The responses to the impulses were measured in corresponding perpendicular planes and used to calculate the transfer functions. Unlike the structural problems that were cited in the background section of this dissertation, a reaction sought after in either the X-plane or the Y-plane in this problem requires transfer functions from both the X and Y planes since there is coupling between them in the transfer function matrix.

Then a force representative of one common in an industrial environment was applied with its magnitude known. The response to that force was measured and pre-multiplied by the inverse of the transfer function already collected, thus computing a predicted forcing function.

This general procedure was repeated with a variety of parameters changed in order to determine a set of criteria that must be met in order to obtain accurate results using this method. It is significant to note that the rotor selected has a first bending mode natural frequency at 2100 CPM. So, it was important to include impulse testing at speeds below, above,

and at that first critical frequency in order to investigate how well the procedure works when the rotor is considered rigid, flexible, and resonant respectively. Rotors are considered rigid when operating below 70% of the 1st critical and flexible otherwise (Ehrich, 1992).

Another parameter that was varied was the location axially along the shaft at which the responses were measured. The first set of data that was processed computed the transfer functions with responses collected near the spinning disk. In this first set of data, the same response locations were used to measure the responses used to predict the forces. Then other response locations along the shaft were collected and processed in order to quantify error as a function of location. In all cases, the impulses were applied at the spinning disk.

The rotor selected, shown in Figure 21, was horizontally installed with a single disk mounted between bearings in order to be representative of a common industrial pump or fan. Its highest damping factor was tested to be 2.45% at its 1st mode. So choosing to neglect damping in the closed form solution was a reasonable assumption. Figure 21 shows the rotor shaft, the mounted disk, and the numbered location at which the perpendicular impulses were applied using a modal hammer (5) and the locations at which responses were measured (1, 2, 3, 4, 6, 7, 8).

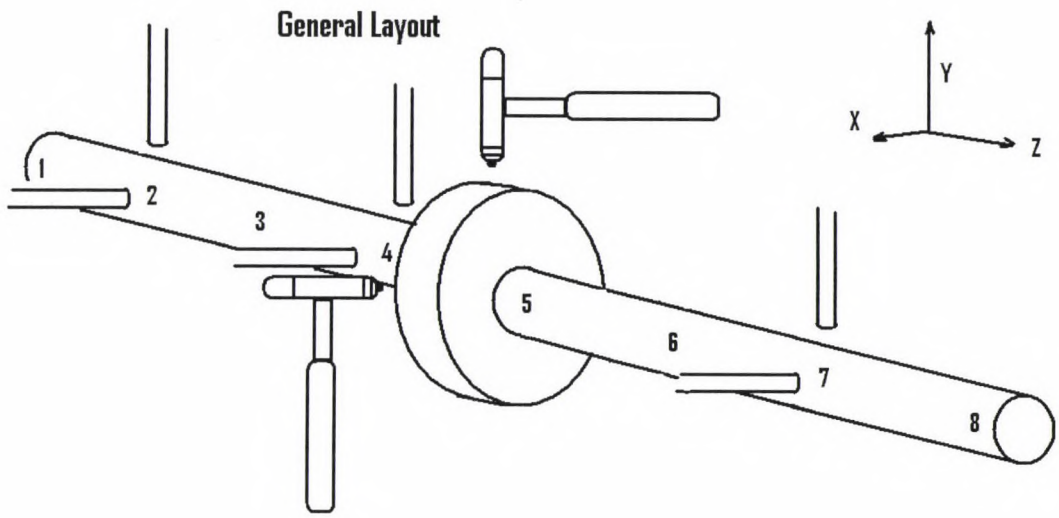

Figure 21 - General Rotor Configuration

The choice for the application of the impulse function was a modal impulse hammer since it is readily available and commonly used in an industrial environment. The response data was measured with non-contact eddy current proximity probes located in both horizontal and vertical planes at several locations axially along the length of the shaft as indicated in Figure 21 by the numbers. These measure shaft displacement vibration directly and do not rely on data transmission through the shaft supporting bushings. Proximity probes are also very commonly used in an industrial setting.

Experimental Procedures

The experimental procedure included several general steps described in more detail in the sections that follow. Those general steps include the setting up the rotor, selecting and installing the measurement system, precision balancing and aligning the rotor shaft and disk, and then applying known loads. Once these steps were complete, a specific procedure was developed, the data collection was performed, and the signal processing was conducted.

Rotor Setup and Applied Loads

The rotor selected was a Bently Rotor kit supplied to Colorado State University by Bently-Nevada Corporation and was set up as shown Figure 22. The rotor is driven by a variable speed motor and connected with a flexible coupling.

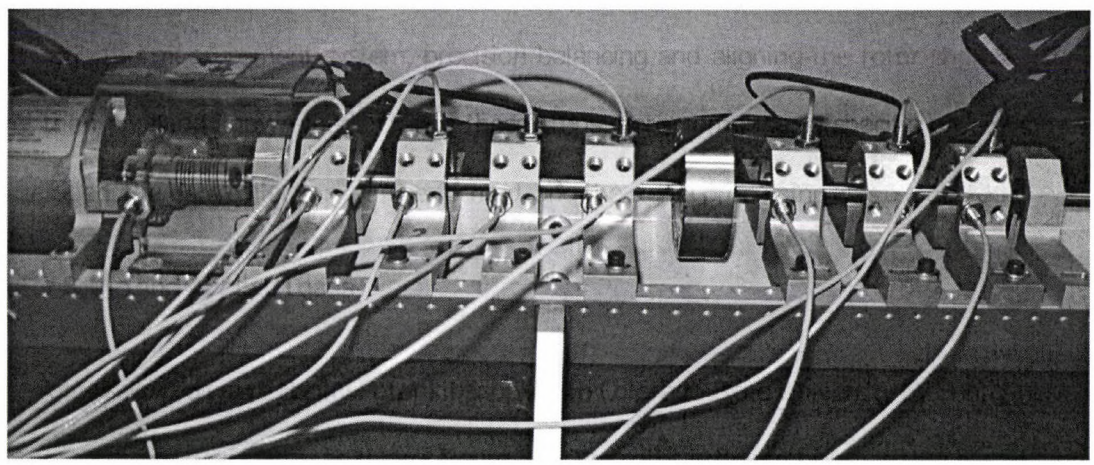

Figure 22 - Bently Nevada Rotor Kit – Side View

In Figure 22 the variable speed motor can be seen at the far left. Immediately to its right is the flexible coupler and then one of the two bushings. Then four pairs of proximity probes are installed. Just to the right of those probes is the spinning disk. Then three more pairs of probes are installed. Finally, at the far right is the second of the two supporting bushings. A top view of the rotor kit is shown in Figure 23.

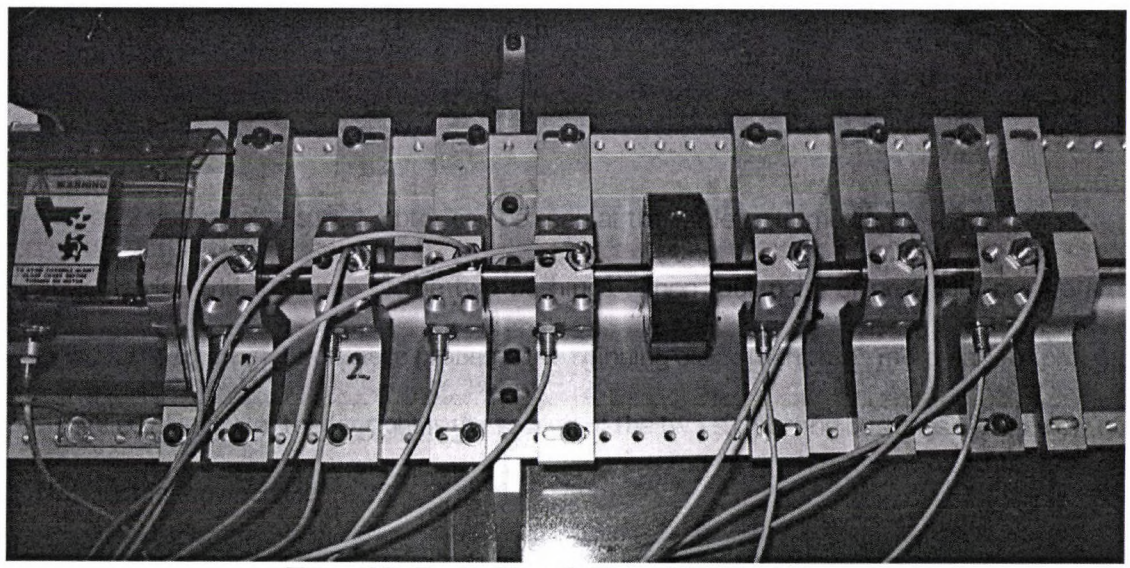

Figure 23 - Bently Nevada Rotor Kit – Top View

Figure 24 shows a close-up of the flexible coupling and the left support bushing.

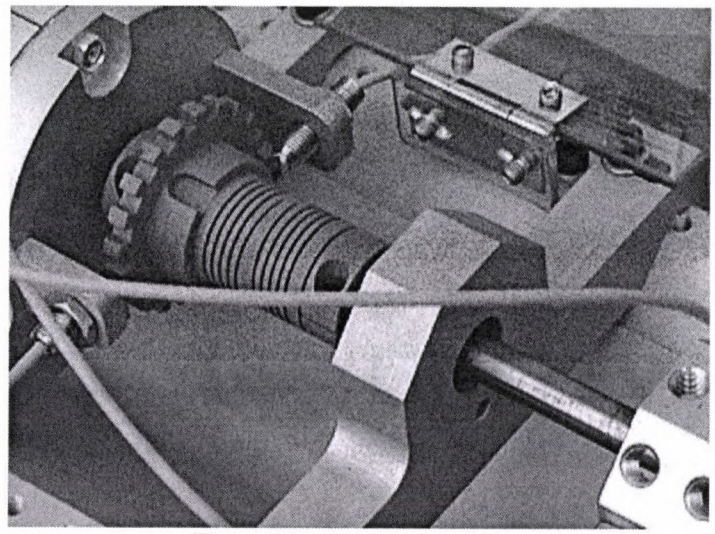

Figure 24 - Flexible Coupling

The rotor was supported at each end by oil impregnated bushings as shown in Figure 25, which is a close-up of the right hand bushing.

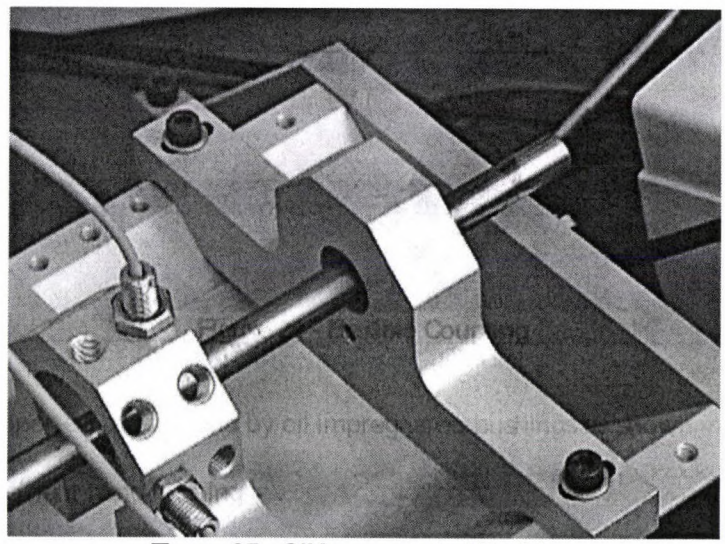

Figure 25 - Oil Impregnated Bushing

The total shaft length was 22 inches and the center to center distance between bearings was 18 inches. The shaft diameter was 3/8 inches. The rotor used included only a single flywheel disk installed at the center between the bearings. The disk was 3 inches in diameter and 1 inch long. It has 16, 3/16 inch diameter holes drilled around the face of the disk near the outside edge.

These holes, shown in Figure 26, were used to install balance weights used for both minimizing the existing loads, and for applying the known unbalance loads.

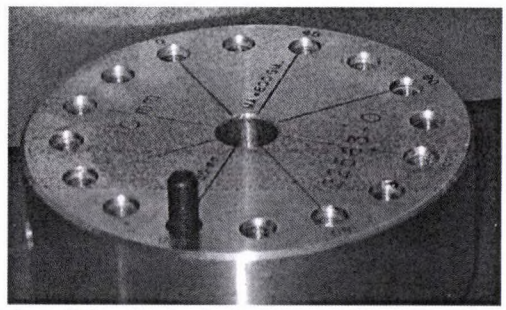

Figure 26 - Balancing disk with imbalance weight shown prior to installation

The alignment was checked and a precision balance performed. The balance corrections were made until any further correction resulted in no improvement to the balance quality.

The known load applied was an unbalance force. The unbalance force was achieved by installing 1.6 grams at a radius of 1-3/16 inch, in the form of screws as shown in Figure 27. The weight was divided in half and the two halves installed opposite each other on both faces of the disk as shown in Figure 27.

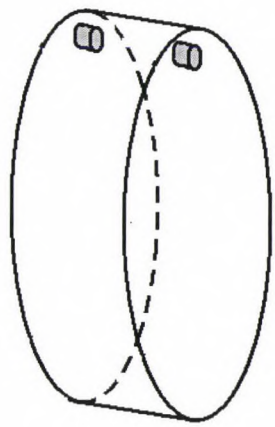

Figure 27 - Installed Unbalance Weights

This was done to ensure that only a radial mass unbalance force was applied and that no couple unbalance, as shown in Figure 28 was induced. Couple unbalance is one where there is an even distribution of mass about the geometric center, but there is a mass distribution such that a force couple exists, causing a out-of-phase wobble from end to end on a rotor. The unbalance force was applied at a variety of different operating speeds for the experiment by using the adjustable speed motor. The speed range selected for experiments and the calculations was 500 RPM to 3600 RPM.

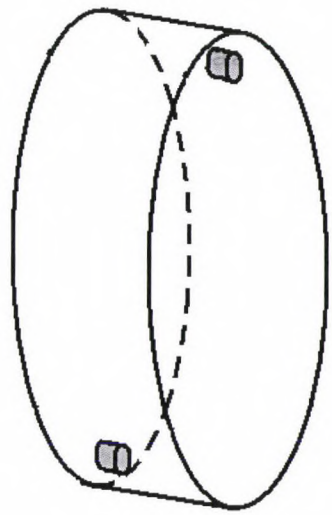

Figure 28 - Couple Unbalance

Instrumentation Setup

A Sony PC208Ax Digital recorder, shown in Figure 29, was used to capture data from up to seven proximity probes and one impulse hammer simultaneously.

Figure 29 - Sony Digital Recorder

The small hammer shown in Figure 30 was used for this experiment, and it has 10 mV/lbf sensitivity.

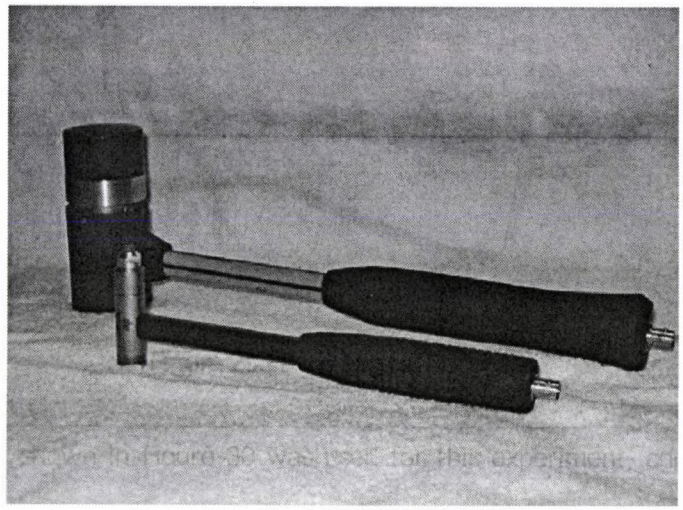

Figure 30 - Modal Impulse Hammers

Fourteen proximity probes, each with 200 mV/mil sensitivity, were installed equally spaced along the length of the shaft as shown in Figure 31.

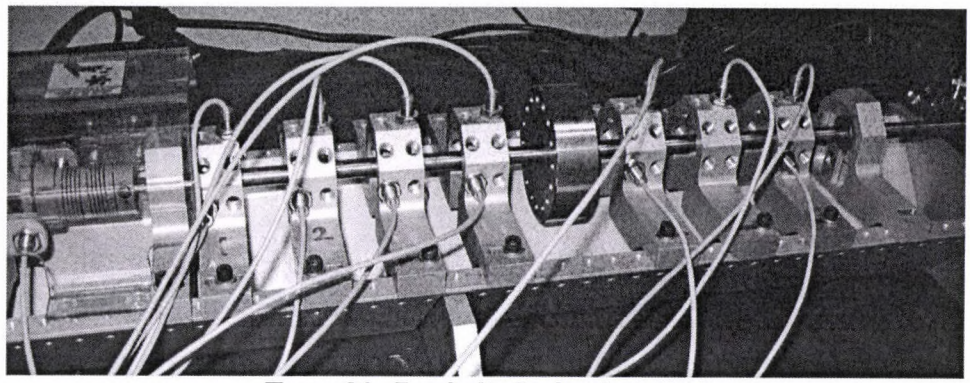

Figure 31 - Proximity Probes Installed

As shown in Figure 32, half of the probes were installed in a vertical direction, and the other half were installed in the horizontal plane.

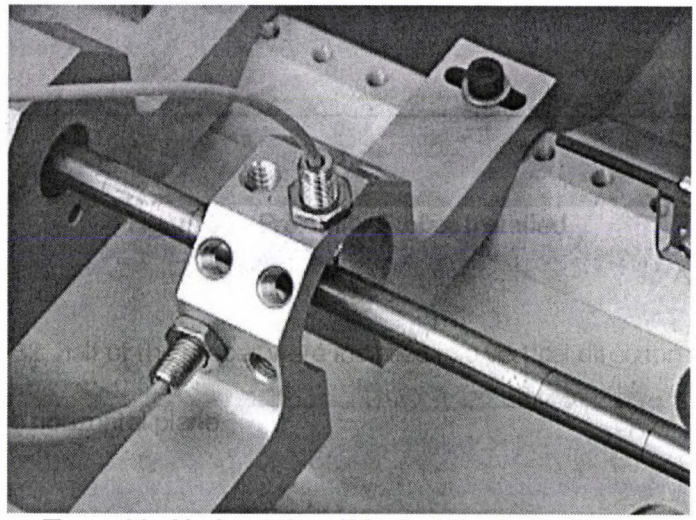

Figure 32 - Horizontal and Vertical Proximity Probes

Figure 33 repeats the general layout of the specific impulse and response measurement locations used for analysis.

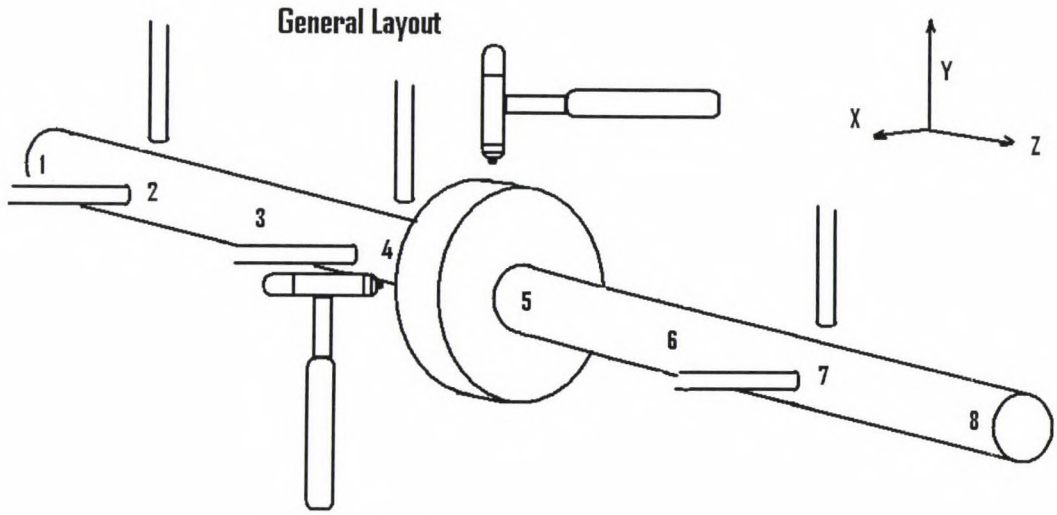

Figure 33 - General Sensor Layout

Note in Figure 33 that the location numbered 5 (at the spinning disk) is the location at which the perpendicular impulses were applied. Also note that, although not shown for clarity purposes in this figure, pairs of perpendicular responses were measured at every other numbered location in the figure. Each of these pairs was used separately in force prediction solutions in order to determine if location along the shaft axially resulted in variable error.

At each response location four transfer functions are collected. First, a hammer strike is applied along the X-axis and a response measured along the X-axis to compute H_{xx}. Second, a hammer strike is applied along the X-axis and a response is measured along the Y-axis to compute H_{xy}. Third, a hammer strike is applied along the Y-axis and a response is measured along the X-axis to compute H_{yx}. Finally, a hammer strike is applied along the Y-axis and a response measured along the Y-axis to compute H_{yy}.

Specific Experimental Procedure

1) Minimize internal forces

    a. Rotor was precision balanced and aligned.

2) Collect a total of 28 transfer functions while the rotor is not spinning. Collect four transfer functions at seven response locations along the shaft. This step is done in order to show that methods, previously researched and cited in the background section of this dissertation, for force prediction on structural vibration systems are not applicable to this rotating system.

    a. With the rotor stopped, an impulse was applied with the modal hammer at the center of the disk in the vertical (Y) direction and all 7 response measurements in the vertical (Y) plane were recorded simultaneously. A total of 6 impulses were applied so that 6 samples were available to use in linear spectral averaging.

    b. With the rotor stopped, an impulse was applied with the modal hammer at the center of the disk in the vertical (Y) direction and all 7 response measurements in the horizontal (X) plane were recorded simultaneously. A total of 6 impulses were applied so that 6 samples were available to use in linear spectral averaging.

    c. With the rotor stopped, an impulse was applied with the modal hammer at the center of the disk in the horizontal (X) direction and all 7 response measurements in the horizontal (X) plane were recorded simultaneously. A total of 6 impulses were applied so that 6 samples were available to use in linear spectral averaging.

d. With the rotor stopped, an impulse was applied with the modal hammer at the center of the disk in the horizontal (X) direction and all 7 response measurements in the vertical (Y) plane were recorded simultaneously. A total of 6 impulses were applied so that 6 samples were available to use in linear spectral averaging.

3) Collect a total of 84 transfer functions while the rotor is spinning. Collect four transfer functions at seven locations while the shaft spins at each of three different speeds: one at which the rotor is considered rigid (1000 RPM), one at which the rotor is considered resonant (2000 RPM), and one at which the rotor is considered flexible (3600 RPM).

   a. The rotor was operated at three speeds, 1000, 2000, and 3600 RPM, and the hammer impulses were applied at each speed as described in Steps 2a – 2d.

4) Since the responses to the impulses applied while the rotor is turning will be complete response data – meaning that the response will have both a reaction to the impulse applied and a reaction to the operating forces – steady state operating data is required in order to be able to subtract that steady state operating data from the complete impulse response data.

   a. An additional one minute of data was recorded at each impulse speed in order to be used to "clean" the complete response data of the steady state operating data leaving only the impulse response. This is described more fully in the signal processing section.

5) Install the unbalance weight and measure the vibration responses at the seven locations and in two perpendicular directions.

   a. A 1.6 gram weight was then installed off center on the disk and the rotor spun between 500 RPM and 3600 RPM.

b. Data were collected by recording one minute every 100 RPM at a sampling rate of 12,000 Hz at all seven locations in the horizontal (X) direction simultaneously.
c. Data were collected by recording one minute every 100 RPM at a sampling rate of 12,000 Hz at all seven locations in the vertical (Y) direction simultaneously.

Signal Processing

Data collected from proximity probes has a significant negative bias voltage. In this case, it is approximately -8.0 volts. So, the "detrend" function in Matlab was used to remove that bias voltage and center the time domain signals around 0 volts. Then, the 200 mV/mil sensitivity was applied and the data converted to displacement measured in mils.

Data from the ICP modal hammer does not carry a bias voltage into the recorder and therefore the Matlab "detrend" function is not necessary for the modal hammer signal. The 10 mV/lbf sensitivity was applied to the impulse signal and the force amplitude computed.

Since the data are periodic and not random in nature, a linear Fast Fourier Transform spectral function was employed in Matlab for all calculations. Since the sampling rate of the recorder is 12,000 Hz, and the frequency ranges in question are less than 100 Hz, aliasing is not a concern. In general, 6 linear averages were applied to all operating data and transfer functions. A linear spectral average is one in which the time domain record is transformed to the frequency domain using a Fourier Transform. Then that frequency domain record is averaged at equal weight with the remaining samples.

Appendix B and Appendix C present the Matlab code used for signal processing.

Analysis Procedures

The analysis procedures include several steps. First, the transfer function calculations were completed. For the static case, these were straight-forward. But, for the case of imparting an impulse to the spinning shaft, more analysis was required. This response to the impulse was a complete response, a combination of the response to the impulse and a response to the operating shaft. So, the two needed to be separated in order to compute an accurate transfer function. Once this was complete, then the inverse force calculations were performed.

Transfer Function Calculations and Matrix Assembly

Once the Fourier Transform is applied to the impulse and response functions, the transfer functions for the all cases were computed as listed in Table 1. In Table 1, $F_X(\omega)$ and $F_Y(\omega)$ are the Fourier transforms of the impulses applied along the x and y axes respectively. $X_i(\omega)$ and $Y_i(\omega)$ are the Fourier transforms of the vibration responses at location i (where i = the measured response locations 1, 2, 3, 4, 6, 7, 8) along the x and y axes respectively. Location 4 was selected as the primary location for measuring responses used for force prediction because it is located closest in physical proximity to the location at which the impulses were applied. The hammer impulses were always applied at the disk location 5. $H_{XX}(\omega)_i$, $H_{YY}(\omega)_i$, $H_{XY}(\omega)_i$, and $H_{YX}(\omega)_i$ are the transfer functions computed from the Fourier Transforms of the force impulses applied and the locations (i) the vibration responses were measured.

Table 1 - Computed Transfer Functions, where i = response locations 1, 2, 3, 4, 6, 7, 8.

Force Input	Response Output	Transfer Function
Horizontal Impulse $F_X(\omega)$	Position i – Horizontal $X_i(\omega)$	$H_{xx}(\omega)_i = \frac{X_i(\omega)}{F_X(\omega)}$
Horizontal Impulse $F_X(\omega)$	Position i – Vertical $Y_i(\omega)$	$H_{yx}(\omega)_i = \frac{Y_i(\omega)}{F_X(\omega)}$
Vertical Impulse $F_Y(\omega)$	Position i – Vertical $Y_i(\omega)$	$H_{yy}(\omega)_i = \frac{Y_i(\omega)}{F_Y(\omega)}$
Vertical Impulse $F_Y(\omega)$	Position i – Horizontal $X_i(\omega)$	$H_{xy}(\omega)_i = \frac{X_i(\omega)}{F_Y(\omega)}$

Before the transfer functions could be computed using the complete impulse response data, collected by applying an impulse to the shaft with a modal hammer while it was spinning, the steady state operating data had to be removed. If it were not, the steady state operating data would contaminate the transfer function and cause extremely high matrix condition numbers at the current operating speed.

For example, the complete impulse response data to the impulse force input was collected along the x-axis at location 4. This complete impulse response data carries both the response to the impulse function and the response to steady state operation. The complete response is shown in Figure 34.

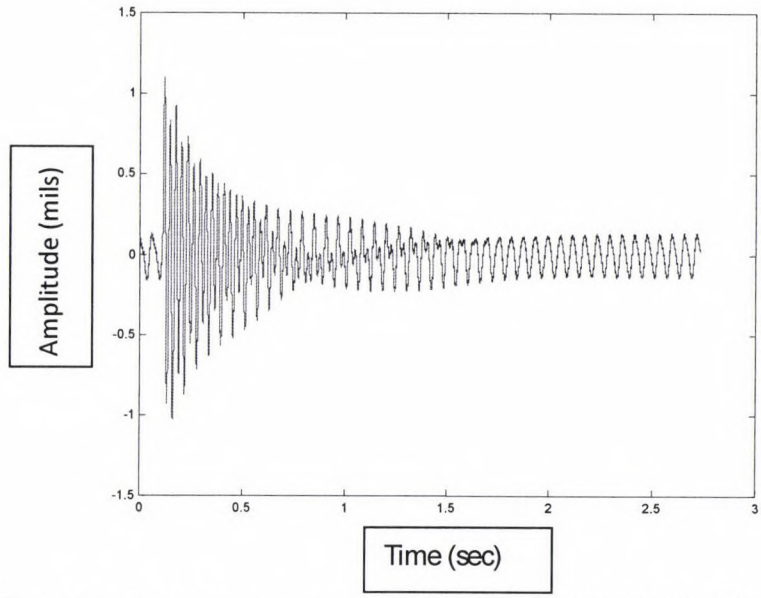

Figure 34 – Complete Impulse Response Data at 1000 RPM in Time Domain

The steady state operating data, collected after the ring down resulting from the applied impulse was complete, was synchronized with the samples that included the impulses. Synchronizing the two signals means to adjust their timing so that they are "in-phase".

Once this synchronization was achieved, the operating data were simply subtracted from the impulse data in the time domain in order to leave only the response to the impulse. The two signals, the steady state operating data signal and the complete impulse response signal, are shown synchronized in Figure 35.

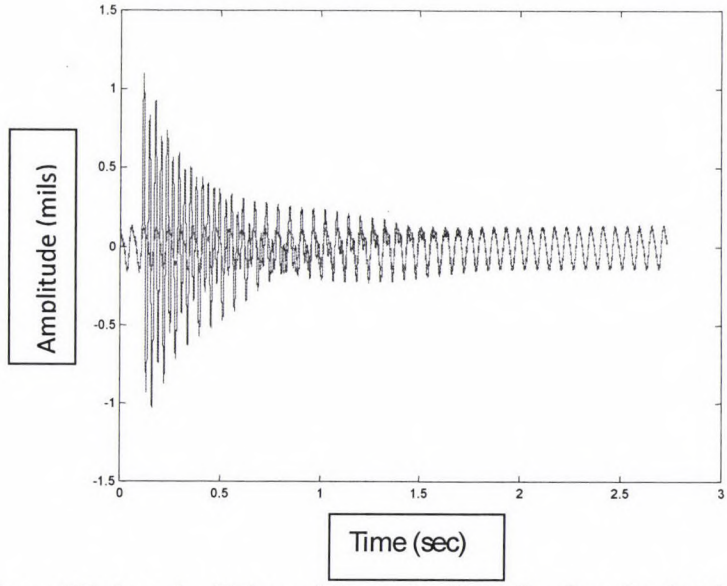

Figure 35 - Impulse Data and Operating Data Synchronized at 1000 RPM

Figure 36 shows the impulse function after being "cleaned" of the operating data.

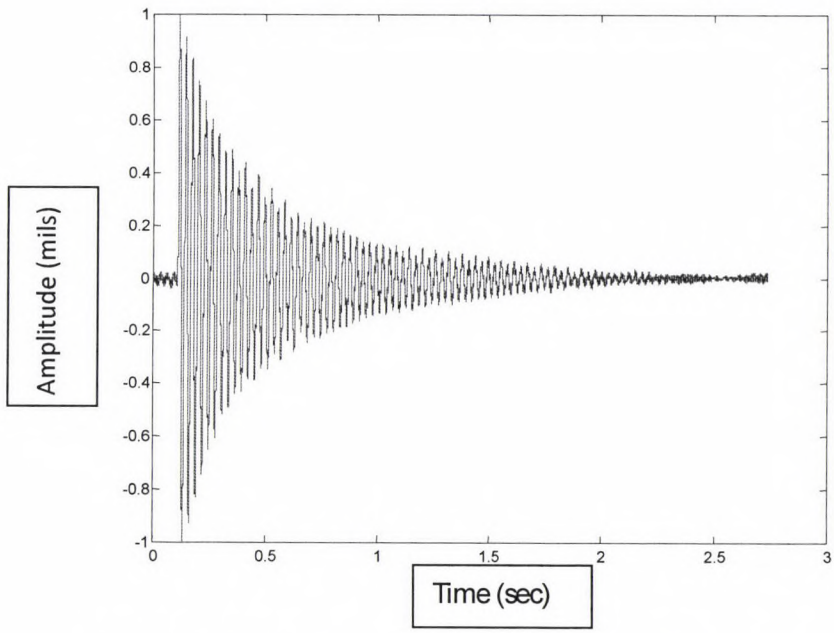

Figure 36 - Impulse Data "Cleaned" of 1000 RPM Operating Data

Next the response functions were computed as indicated in Table 1.

Once all of the transfer functions were computed, the transfer function matrices for each location were assembled as shown in Equation 44.

$$H(\omega) = \begin{bmatrix} Hxx & Hxy \\ Hyx & Hyy \end{bmatrix} \tag{44}$$

Figure 37 and Figure 38 depict the four transfer functions that were determined while operating at 1000 RPM and measured at location 4.

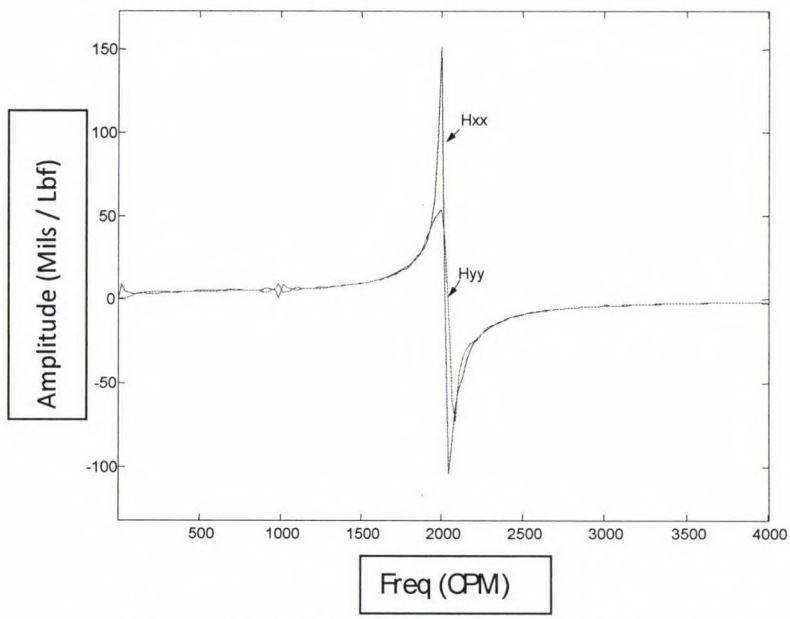

Figure 37 - Hxx and Hyy Transfer Functions at 1000 RPM

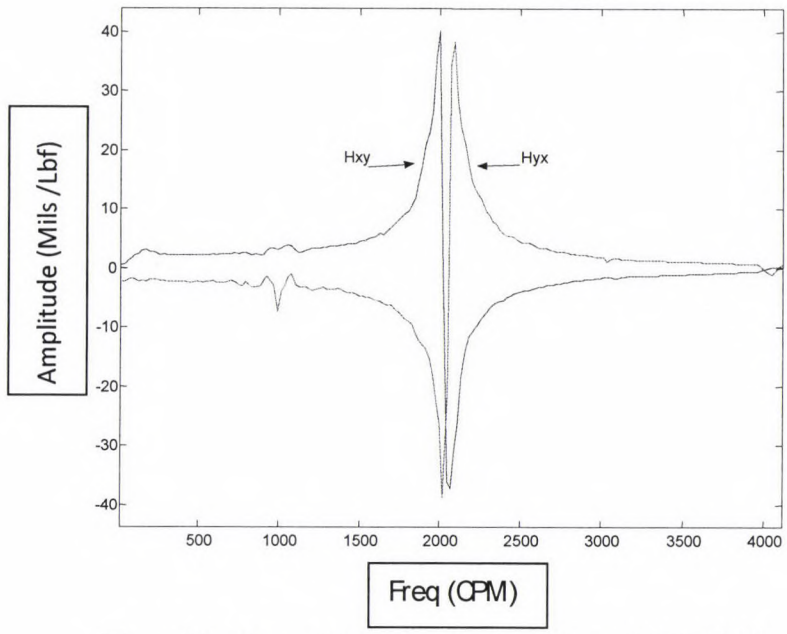

Figure 38 - Hxy and Hyx Transfer Functions at 1000 RPM

Next the unbalance weight was applied, the data recorded, and the response matrices were assembled as shown in Equation 45.

$$A(\omega) = \begin{pmatrix} X(\omega) \\ Y(\omega) \end{pmatrix} \tag{45}$$

Force Calculations Using the Pseudo-Inverse Method

Then the transfer function matrix was inverted and pre-multiplied with the response matrix in order to compute the forces as found in Equation 46.

$$F(\omega) = H^{-1}(\omega)A(\omega) \tag{46}$$

Since the number of responses, shown in Equation 45, measured and used for force prediction is two, which is the same as the number of forces desired, the system is not over-determined, and the matrix is square and invertible in a traditional manner (Ewins, 2000).

However, conditions may exist that do require an alternative method in order to invert the transfer function matrix. Since testing was carried out at or near a resonant frequency, the response matrix may be ill conditioned. At or near resonant frequencies, the amplitudes of the frequency response function may be extremely high, while at the anti-resonant frequencies the amplitudes may be extremely low. These phenomena cause ill-conditioning and calculation errors. (Fabunmi, 1986)

One method used to predict ill conditioning is the calculation of the matrix condition number. The condition number is the ratio of the largest singular value in the singular value decomposition matrix to the lowest. If this number becomes large, then the matrix is ill conditioned (Desanghere & Snoeys, 1985). So, in all cases the condition number was computed and plotted versus frequency in order to determine the ranges where ill conditioning exists.

If ill conditioning exists, an alternative method for matrix inversion is available and a solution can still be found. A pseudo-inverse function can be computed by using singular value decomposition (Strang, 1988). If Equation 47 gives the singular value decomposition of a matrix A, then the pseudo-inverse of A, which is denoted A^{+}, is found with Equation 48 (Strang, 1988). In these equations, Σ is a matrix that has the singular values of A on its diagonal, and the reciprocals of the singular values of A are found on the diagonal of Σ^{+} where the + refers to the pseudo inverse of the matrix.

$$A = Q_1 \Sigma Q_2^T \tag{47}$$

$$A^+ = Q_2 \Sigma^+ Q_1^T \tag{48}$$

One problem that arises from any inverse problem is that its solutions are not unique. Physically, this occurs when more than one combination of forces can put the system into the same measured response (Ewins, 2000). Practically, this is handled by making an estimation of a reasonable solution prior to starting the analysis. This is relatively easy to do in applications to industrial machinery because the locations of the disks and bearings are known from the specifications of the machinery, and the operating speeds are known by measurement with a tachometer.

The data selected for analysis includes the response functions listed in Table 1 collected with the rotor at rest, and then spinning at 1000, 2000, and 3600 RPM. The response locations selected for this analysis were 2, 4, and 7. These locations are depicted in Figure 33. Though the primary location studied was location 4, analysis at locations 2 and 7 will give an indication of the level of influence axial location has on the accuracy of the results.

The operating speeds used for the force predictions are 600, 800, 1000, 1100, 1500, 2200, 3200, and 3600 RPM. These speeds were chosen because of their proximity to the speeds at which the impulses were applied, or their frequency relative to the first natural frequency. The operating speeds at 600, 800, 1100, and 1500 RPM were chosen because they are close to the 1000 RPM speed at which some of the impulses were applied. The operating speed at 2200

RPM was chosen because it is at one of the rotor resonance frequencies. The operating speeds at 3200 and 3600 RPM were chosen to be near the impulses applied at 3600 RPM.

Results

This section includes a summary of the results and a discussion of possible sources of error. It also includes a listing of a set of criteria that will ensure the most acceptable predictions that can be obtained using this method. This section concludes with an analysis of the limitations of these force prediction methods.

Summary of Results

There are two parts to every force prediction solution, the forcing frequency and amplitude. In every case, the frequency prediction is excellent and is less than the spectral resolution. In all cases, the sampling rate for data collection was 12,000 Hz, and the number of samples collected was 32768. Dividing this frequency range by the number of samples gives the frequency resolution at 0.366 Hz, or 22.0 CPM. Since the force prediction method always placed the predicted frequency in the appropriate frequency bin in the Fourier Transform spectrum, the margin of error was always a function of the frequency in question. For example at the lowest predicted frequency, 600 CPM, the margin of error was a function of that predicted frequency and the frequency resolution, 22 CPM. So in this case, the largest possible error in frequency was less than 3.66%. In the case where the predicted frequency was 3600 CPM, the 22 CPM resolution gives a largest possible margin of error at 0.6%. At the predicted frequency of 1100 CPM, the largest possible error is 2% with the 22 CPM resolution. In addition, the force

prediction method never returned a harmonic, which is correct for an unbalance force. This is exceptional considering that in many cases, the response data did contain harmonics.

Note in Figure 39 the response measured at location 2 shows two significant frequencies, the running speed frequency caused by the unbalance force, and a harmonic of that force most likely caused by a response system aggravating condition, such clearance in the bushing. Note that all spectral plots use cycle per minute (CPM) units to measure frequency.

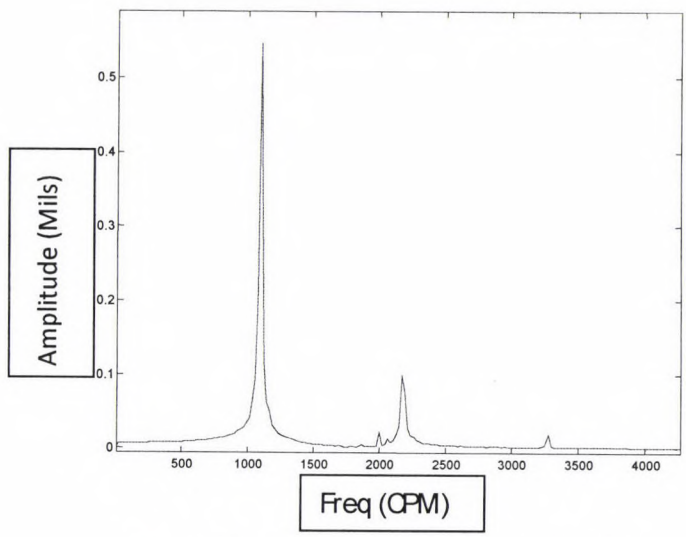

Figure 39 – Y-Dir Response, Pt 2, 1100 RPM

The force prediction extracted from that response is shown in Figure 40. It presents only one frequency, the mass unbalance frequency. Mass unbalance generates a single forcing frequency and that is what was predicted, almost without fail for the entire list of tests. Accurate amplitude, however, was far more difficult to achieve.

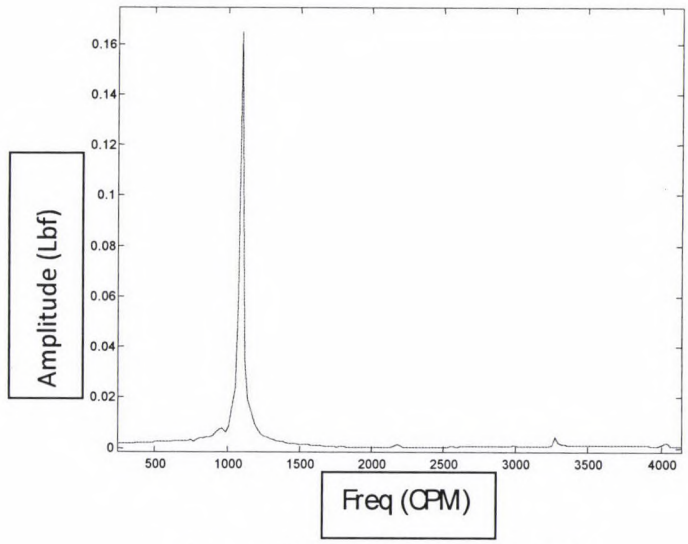

Figure 40 - Y Force, Pt 2, 1100 RPM

The best amplitude results come from the tests at which the impulse force was applied at 1000 RPM, and the force predicted at a response speed of 1100 RPM. In these tests, the speed at which the impulse force was applied was close enough to the unbalance response speed that the response matrices are similar. And, it was not so close as to fall within a range of high matrix condition number. Figure 41 and Figure 42 give the vibration response and force prediction respectively for an unbalance applied at 1100 RPM with the unit impulse applied at 1000 RPM, all at position seven. Note that the force prediction algorithm computed 0.15 lb, while the actual unbalance force was 0.144 lb. This result is less than 1% error.

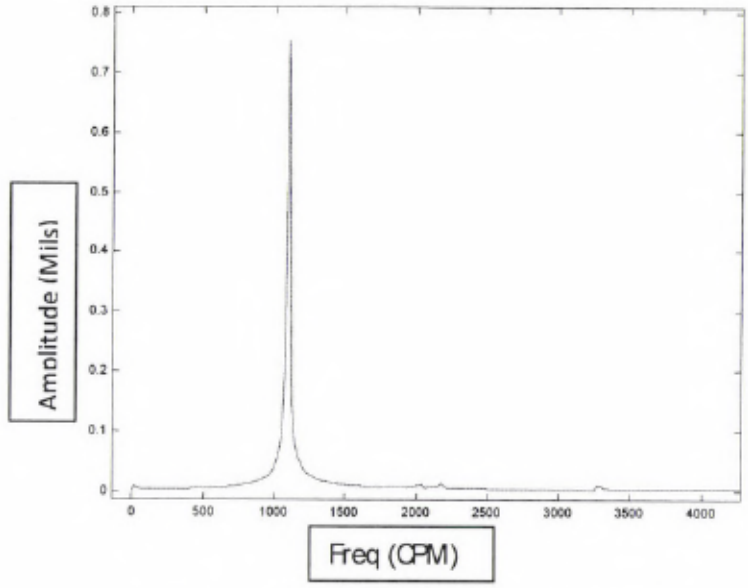

Figure 41 - X-Dir Response, Pt 7, 1100 RPM

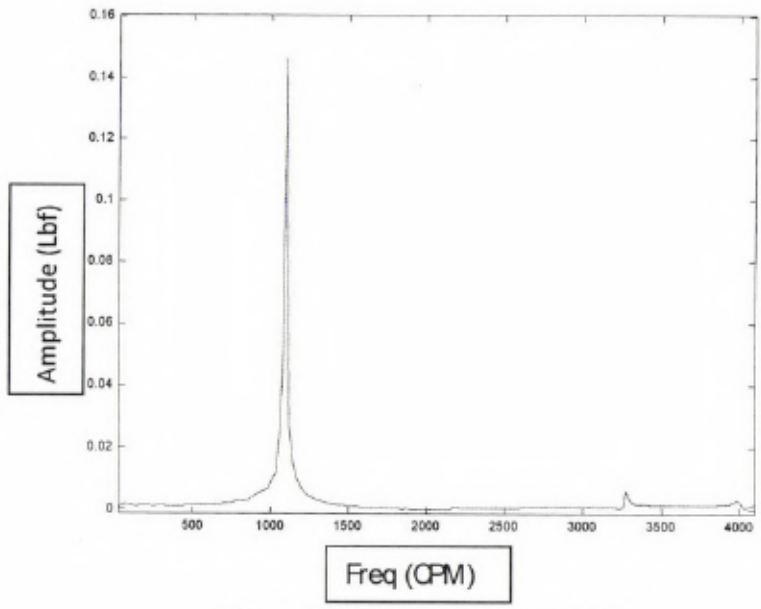

Figure 42 - X Force, Pt 7, 1100 RPM

Many of the scenarios were not nearly as accurate. Forces predicted from the static response functions were extremely inflated and inaccurate. Predictions that included either an impulse or response frequency at or near the shaft critical speed also had poor accuracy. Finally, those

with a large variation between the impulse and response speeds were also outside an acceptable accuracy limit.

Figure 43 repeats the details of the impact locations and response positions.

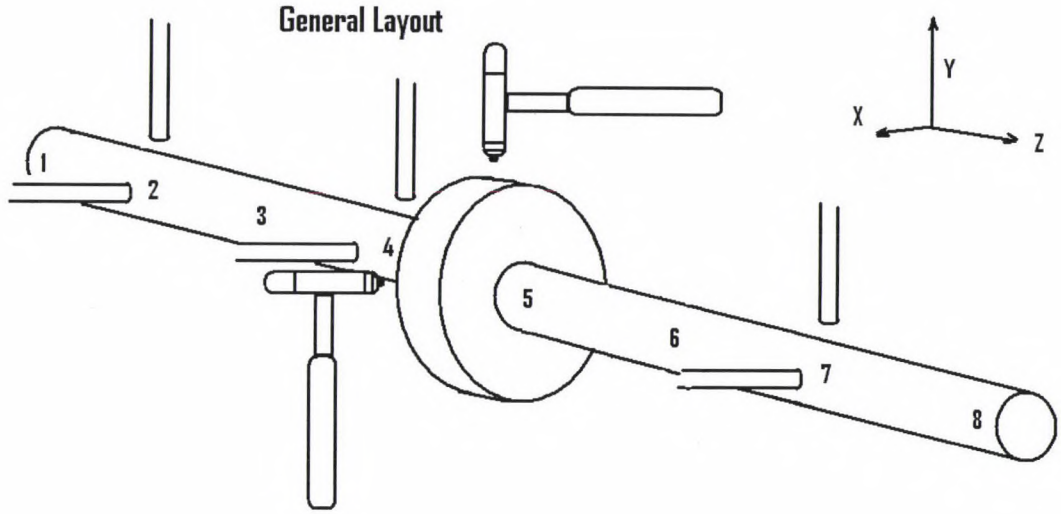

Figure 43 - General Rotor Configuration and Sensor Layout

Figure 44 gives a summary the results of all of the experiments and data analysis performed. The impact speed is the rotor speed at which the impulse is applied using the modal hammer (1000, 2000, and 3600 RPM). The response speed is the rotor speed at which a known unbalance force is applied and techniques used to predict the force. All speeds were measured with a laser tachometer. The impact location is the location at which the hammer impulse was applied – location number 5. The response position is the location of the proximity sensors that were used to measure the vibration responses to the impulses applied as well as the unbalance input. The condition number is a measure of the susceptibility of the transfer function matrix

when an operation, such as inversion, is performed on it. The operating to impact speed ratio is a ratio between the rotor speed at which the response to the known unbalance is measured, and the rotor speed at which the impulse was applied. The X force column is the amplitude of the predicted force at the response location along the X axis. The Y force column is the amplitude of the predicted force at the response location along the Y axis. The columns for percent error present the percent difference between the predicted forces and the actual applied unbalance forces.

Impact Speeds	Response Speeds	Impact Location	Response Position	Condition Number	Oper:Impact Speed Ratio	X Force (lbf)	Y Force (lbf)	Calc Force (lbf)	X % Error	Y % Error
0	1000	5	4	12.7	NA	1.32	0.27	0.12	1009%	123%
0	3600	5	4	14.9	NA	10.45	2.25	1.54	578%	46%
1000	600	5	4	1.1	0.60	0.20	0.03	0.04	362%	-30%
1000	800	5	4	1.2	0.80	0.05	0.09	0.08	-34%	14%
1000	1000	5	4	3.0	1.00	0.13	0.15	0.12	11%	25%
1000	1100	5	4	1.3	1.10	0.10	0.10	0.14	-33%	-33%
1000	1100	5	2	1.3	1.10	0.18	0.17	0.14	24%	15%
1000	1100	5	7	1.1	1.10	0.15	0.17	0.14	1%	17%
1000	1500	5	4	1.1	1.50	0.09	0.18	0.27	-67%	-31%
1000	3600	5	4	1.3	3.60	0.57	0.81	1.54	-63%	-48%
2000	1000	5	4	1.6	0.50	0.07	0.08	0.12	-40%	-34%
2000	2200	5	4	1.9	1.10	0.27	0.23	0.58	-54%	-60%
2000	3600	5	4	1.8	1.80	0.61	0.76	1.54	-61%	-51%
3600	1000	5	4	1.5	0.28	0.05	0.09	0.12	-57%	-26%
3600	2500	5	4	1.5	0.69	0.50	0.22	0.74	-33%	-71%
3600	3200	5	4	1.8	0.89	0.39	0.43	1.22	-68%	-65%
3600	3600	5	4	3.3	1.00	0.05	0.04	1.54	-97%	-98%

Figure 44 - Summary of Results

Error Analysis

The error analysis begins with a review of the repeatability of the transfer functions, as well as the causality between the force impulse input and the vibration response output. It then discusses error within the results.

Figure 45 displays spectra of the six transfer functions used to compute the average transfer function for the force impulse applied along the x-axis and the response also measured along the x-axis. These six transfer functions were collected while the rotor was spinning at 1000 RPM. It should be noted that these transfer functions were not "cleaned" of the steady state operating data so that any estimation of repeatability could not be attributed to the synchronizing and "cleaning" process.

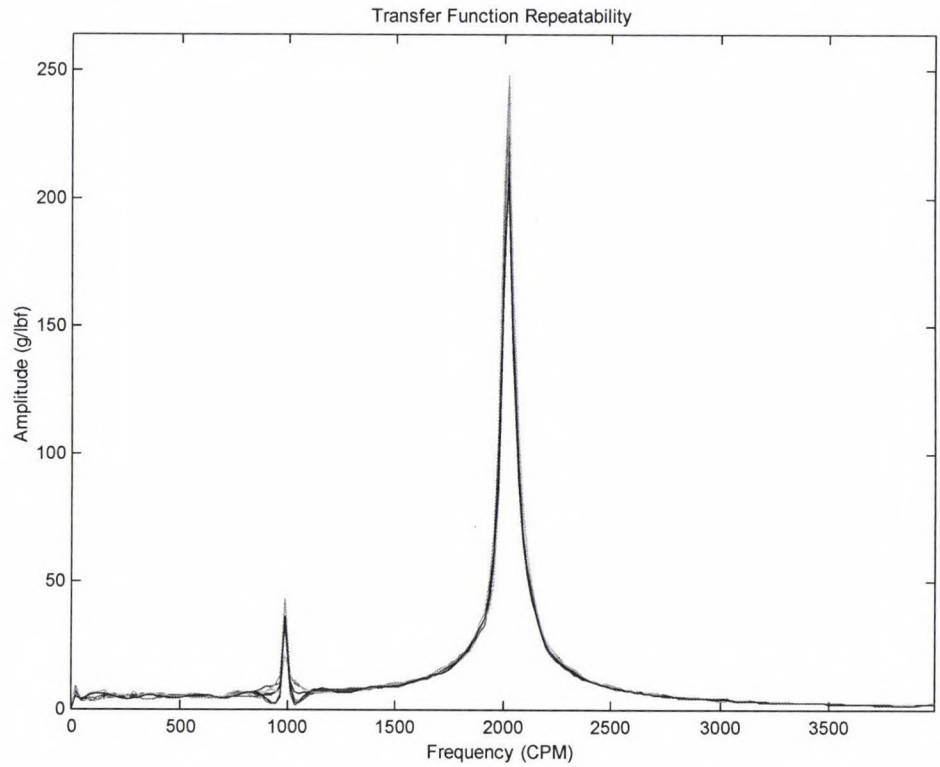

Figure 45 - Transfer Function Repeatability

It is clear that in Figure 45, the repeatability of the transfer functions is very good. In the figure, the least repeatability occurs in and around 1000 CPM, which is the frequency at which the rotor was spinning when the impulse was applied.

A quantitative assessment of the repeatability was calculated by computing the standard deviation of the amplitude of the transfer functions. This calculation was performed and is displayed as a percentage of the average value in Figure 46. In this figure, the deviation is expressed as a percentage of the average value versus frequency measured in CPM.

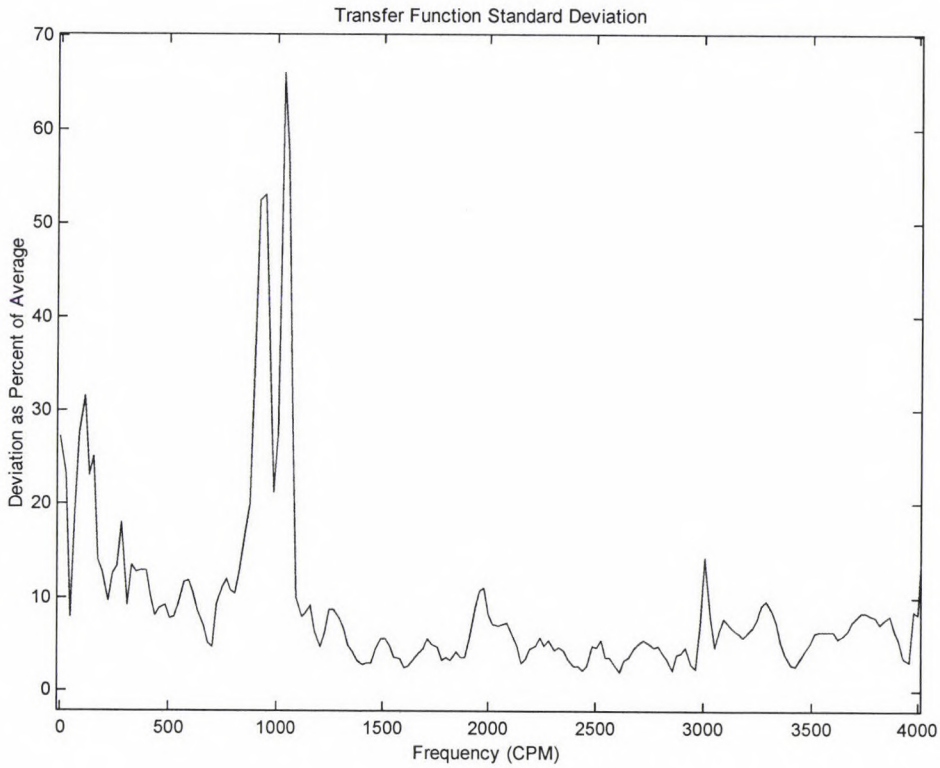

Figure 46 - Transfer Function Standard Deviation as Percent of Average Value

Note in Figure 46 that the highest deviation occurs at the frequency coincidental with the rotor speed at which the impulse was applied. Aside from low frequencies (< 300 CPM), the maximum deviation is less than 10% at frequencies away from 1000 CPM. This is a good outcome and lends confidence in the reliability and accuracy of the method because of the excellent repeatability.

Figure 47 depicts this same standard deviation plot zoomed in to the area near 1100 CPM, the speed at which the best force amplitude prediction results were obtained. This plot shows that the standard deviation at 1100 CPM is 9.8%, which is less than the average amplitude prediction error for this frequency. Further support for the criteria for acceptable results is gained by the fact that the deviation drops significantly as the frequency in questions deviates away from the rotor speed at which the impulses were applied.

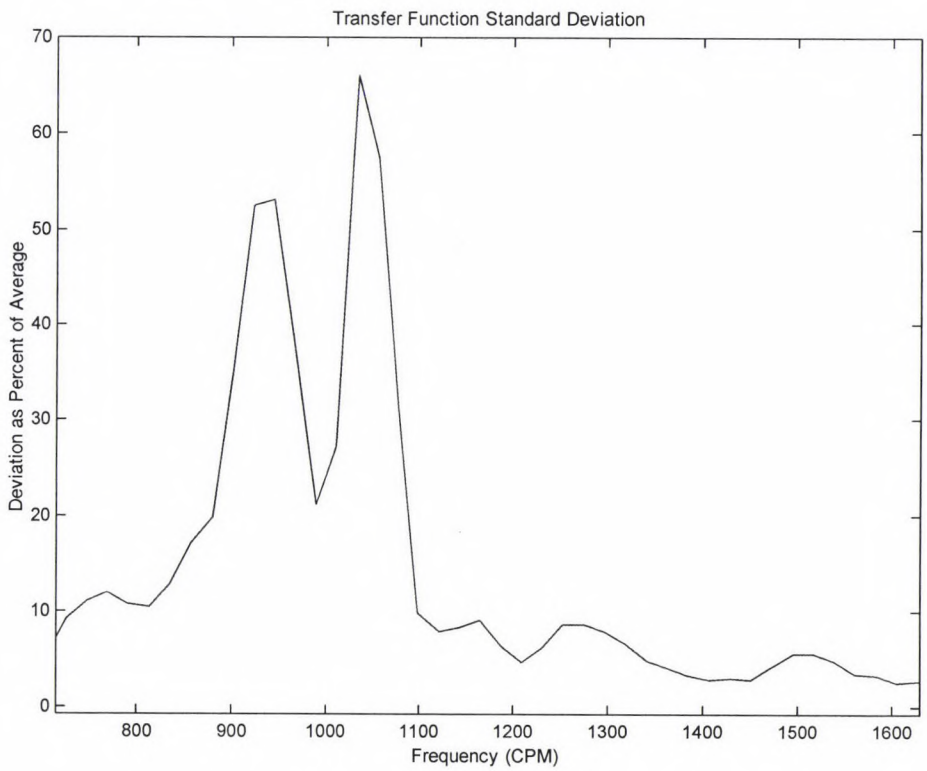

Figure 47 - Zoomed Transfer Function Deviation

Another measure of data validity in the arena of modal testing is the coherence function. Prior to computing the coherence function though, the frequency range excited by the applied hammer impulse function is checked to ensure that the hammer tip selected excites a frequency

range high enough to cover the range of interest. This is done by computing the Fourier Transform of the hammer impulse function and noting the frequency range that is excited. Typically, the acceptable range is selected as one in which at least 70% of the full scale impulse amplitude is contained.

Figure 48 shows the Fourier Transform of the impulse function. In this plot, the amplitude of the impulse (lbf) is plotted versus frequency (CPM). Then, amplitude equal to 70% of the full scale impulse amplitude is marked and the corresponding frequency range depicted.

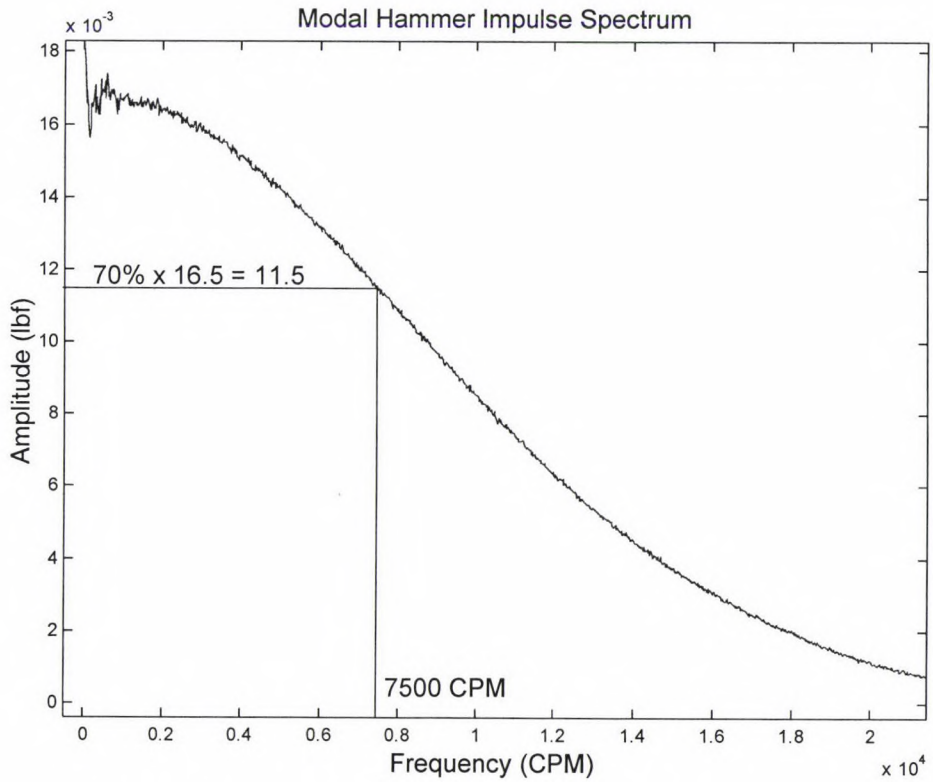

Figure 48 - Modal Hammer Impulse FFT Spectrum

The acceptable frequency range using this criterion is 7500 CPM. Since the frequency range of interest is less than 4000 CPM, this measured range is adequate.

The best indicator of the level of causality in modal testing is the dimensionless coherence function (Bendat & Piersol, 1993). It is computed using the six samples of data used for averaging the transfer functions. It is calculated using Equation 49 (Bendat & Piersol, 1993) where COH is coherence, and $H(\omega)_1$ and $H(\omega)_2$ are transfer functions defined in the next equations.

$$\mathrm{COH} = \frac{\mathrm{H}(\omega)_1}{\mathrm{H}(\omega)_2} \tag{49}$$

The transfer functions, $H(\omega)_1$ and $H(\omega)_2$, used in the coherence calculation are defined in Equations 50 and 51 (Bendat & Piersol, 1993).

$$H(\omega)_1 = \frac{G_{AF}}{G_{AA}} \tag{50}$$

$$H(\omega)_2 = \frac{G_{FF}}{G_{FA}} \tag{51}$$

In these equations, G_{FF} and G_{AA} are the auto spectra of the Fourier Transforms of the force impulses input and vibration responses output respectively. G_{AF} and G_{FA} are the cross spectra between the Fourier Transforms of the force impulses input, $F(\omega)$, and vibration responses output, $A(\omega)$. The auto spectra and cross spectra are computed in Equations 51, 52, 53, and 54. Note in these equations that computations for each of the 6 samples included in the average are summed together (Bendat & Piersol, 1993).

$$G_{AF} = \sum_{i=1}^{6}(conj(A(\omega)_i)F(\omega)_i) \quad (51)$$

$$G_{FA} = \sum_{i=1}^{6}(conj(F(\omega)_i)A(\omega)_i) \quad (52)$$

$$G_{AA} = \sum_{i=1}^{6}(conj(A(\omega)_i)A(\omega)_i) \quad (53)$$

$$G_{FF} = \sum_{i=1}^{6}(conj(F(\omega)_i)F(\omega)_i) \quad (54)$$

In practice, an acceptable criterion for coherence is that it should exceed 90% in order to estimate causality (Bendat & Piersol, 1993). Causality, in this case, is the notion that the hammer impulse input is causing the vibration response output.

Figure 49 depicts the coherence (dimensionless) plotted versus frequency (CPM). Note that aside from the low frequencies (<300 CPM), the coherence is at 97% except near the frequency coincidental with the speed at which the rotor was operating when the impulse was applied.

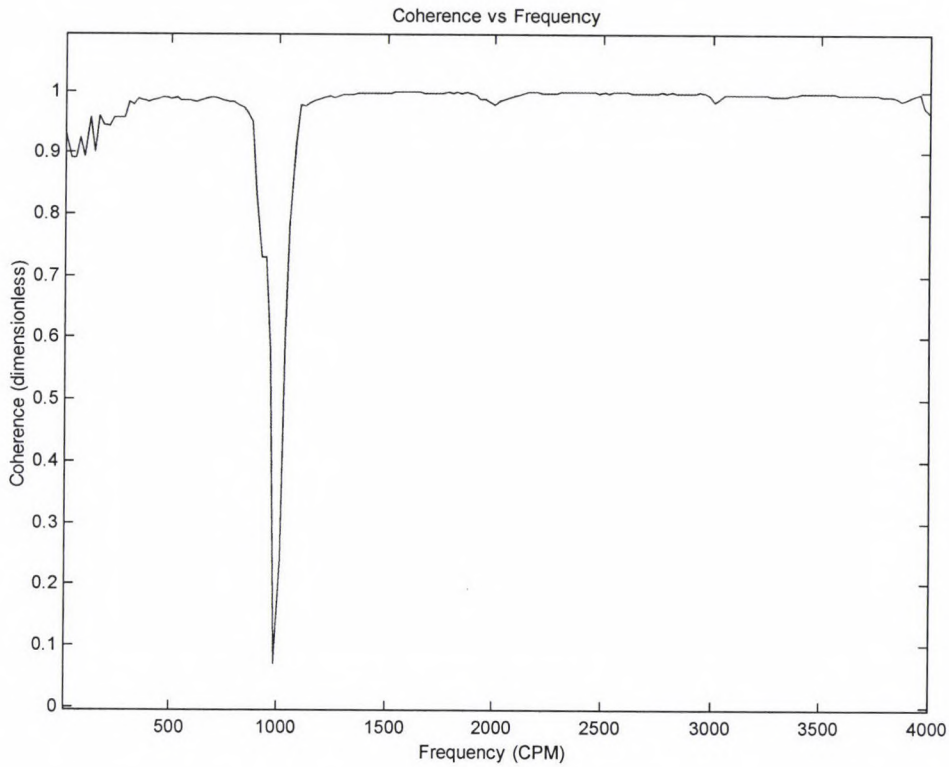

Figure 49 - Coherence Between Impulse Input and Vibration Output

This is not surprising, and in fact it is expected since the complete response function was not cleaned of the steady state operating data. This means that the vibration response measured at 1000 CPM was not caused by the hammer impulse input, but rather by the steady state operating conditions.

Figure 50 shows the same coherence plot zoomed to show the value at 1100 CPM, the operating speed at which the best results were obtained. Note that the coherence at 1100 CPM is at 97.8%.

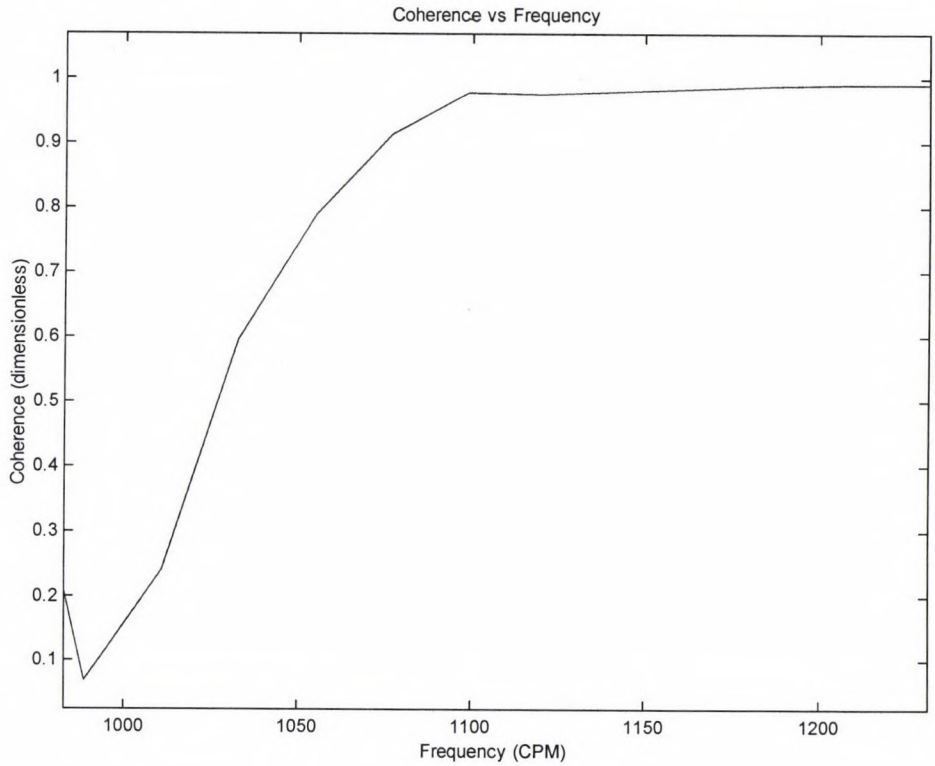

Figure 50 - Zoomed Coherence

The previous discussion shows that the transfer function amplitude data is repeatable well within the average amplitude margin of error. It also shows that the hammer and tip selected were able to excited frequencies above the required frequency range, even when applied to the spinning shaft. It also shows that there is excellent causality between the hammer impulse input, and the vibration response output. The Matlab code used to compute standard deviation and coherence is included in Appendix D. Following is a discussion regarding error within the results.

The results of force prediction from the static impulse transfer functions are so extremely erroneous that they are excluded from this error analysis. As mentioned previously, they were

included in order to show that transfer functions collected while a shaft is idle do not apply to the case of force prediction with a rotating shaft.

Since the rotor is symmetric about both the X and Y axis, one measure of accuracy in the experimental results is to examine the correlation between the force prediction error along the X axis and the force prediction error along the Y axis. So, in order to do this, the data shown in Figure 44 were sorted, and ranked according to absolute magnitude of the force amplitude prediction error along the X-axis. Figure 51 plots the error in force prediction along both the X and Y axes for all of the data points in Figure 44 against the "rank number". The rank number is defined here such that a rank number of "1" refers to the lowest X% error and a rank number of "15" refers to the high error in the X% error column of Figure 44. The data point at rank number 15 is clearly not correlating with the rest of the data. This set is for an operating speed of 600 RPM, and the rotor speed at which the hammer impulse was applied was 1000 RPM. Computing the correlation with this data set gives a value of only 7.8%. Excluding this data point gives a strong correlation of 70.5%. Two reasons are likely the cause of the poor correlation at 600 RPM. First, the difference between the operating speed and the rotor speed at which the hammer impulse was applied is large (40%), which means the dynamics are considerably different between the two frequencies. Second, the force of unbalance, since is varies with the speed squared, is so low at the slow speed of 600 RPM that the expected force is dominated by the other forces that can cause running speed frequency vibration such as alignment issues and eccentricities in the motor and coupling. Considering the good correlation for all of the data except for the slow rotor speed of 600 RPM, it is concluded that the Bently Rotor kit is a suitable subject for an axis-symmetric model.

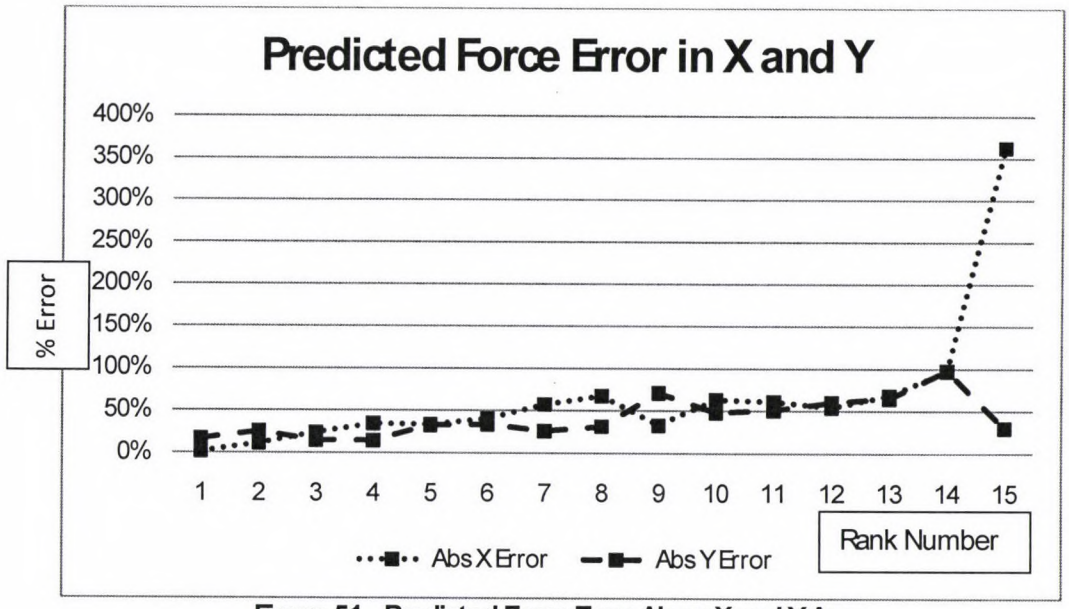

Figure 51 - Predicted Force Error Along X and Y Axes

While there are several factors that cause errors in the force calculation, none have a stronger correlation to those errors than the condition number. To illustrate this, the data of Figure 44 were sorted and ranked according to the average force amplitude prediction error. In each row of Figure 44, this is the average of two numbers, the number in the X% error column and the number in the Y% error column. Figure 52 presents the average percent error and the condition number plotted versus the rank number defined in the same way as it was defined for Figure 51, except that here it is based on the average of the X and the Y error. Note that there are two data points which clearly do not correlate with the rest of the data, the data with rank number 2 and rank number 15. The data set with rank number 2 is one where the operating speed and the rotor speed when the hammer impulse was applied were the same, at 1000 RPM. With these data, the condition number was large (3.0), but the average amplitude error was low (18%). This further proves the point that data with a high condition number are unreliable. The other data point that doesn't correlate is rank number 15. This is the same data point that did not correlate in Figure 51, which is the data set at which the operating speed was 600 RPM, and

the rotor speed at which the impulse was applied was 1000 RPM. In this case the condition number was low (1.1) but the average amplitude error was high at 197%. As mentioned before, it is likely the low dynamic effect of unbalance at that slow speed that causes this discrepancy. Including all of the data sets, the condition number and average amplitude error do not correlate well with a value of 0.26%. But if data sets ranked 2nd and 15th are removed, the computed correlation between the condition number and the average error suggests strong correlation at a value of 70%.

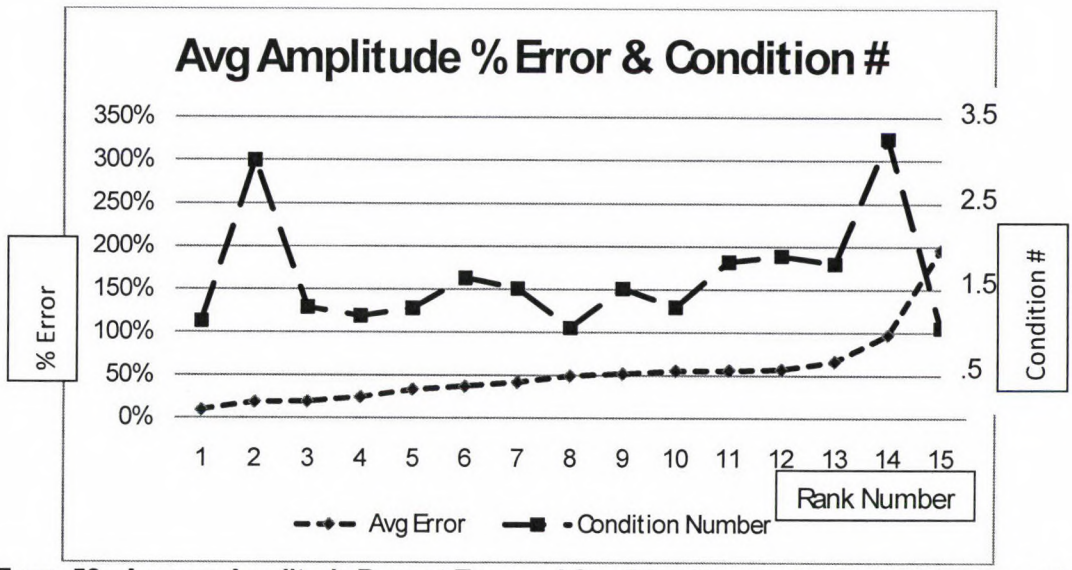

Figure 52 - Average Amplitude Percent Error and Condition Number for Each Measurement

Figure 53 depicts the condition number against frequency, measured in CPM, for the transfer function generated at 1000 RPM.

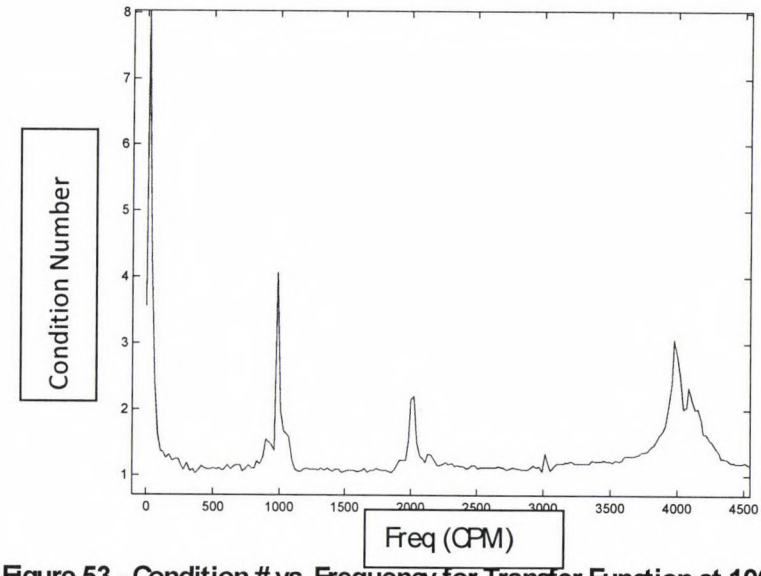

Figure 53 - Condition # vs. Frequency for Transfer Function at 1000 RPM

Note that even with careful signal processing to minimize the influence of the rotor operating speed in the transfer function, the condition number still rises considerably at the operating speed and at its harmonics.

In Figure 54, the condition number is plotted vs. frequency for the impulses applied on the rotor while it was spinning at 3600 RPM. The lowest condition number is more than twice the best condition numbers when the impulse was applied while spinning 1000 RPM. A flexible rotor condition may be negatively influencing this. The rotor is operating above its first critical speed and is considered a flexible rotor with a mode shape significantly affecting shaft displacements. It is likely that the response to a unit impulse may be affected as a result of this influence making the response matrix ill-conditioned at all frequencies.

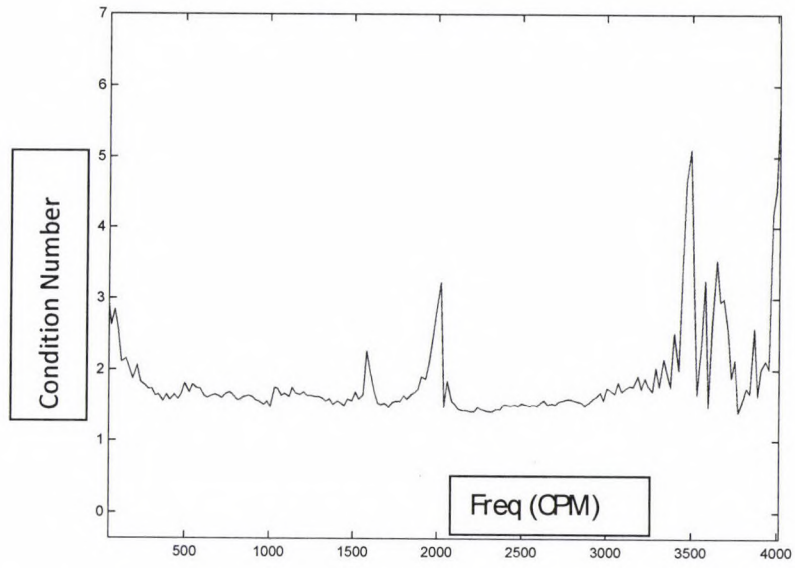

Figure 54 - Condition # vs. Frequency for Transfer Function at 3600 RPM

In addition to the large minimum condition number, there is very poor conditioning at or near the 3600 RPM rotor operating speed at which the impulse was applied. This is due to the difficulty in fully removing the influence of the operating data on the impulse data embedded in the complicated signal. Based on these results in Figure 54, it was expected that force prediction from the 3600 RPM impulse response functions would be poor, and as is shown in the results section, it is.

Figure 55 shows the condition number for the response matrix generated from an impulse applied while spinning at 2000 RPM. Since the rotor is operating near its critical speed at 2100 RPM, it is not surprising to see a high condition number at 2000 CPM. Though the condition numbers at all other frequencies appear to be lower, close inspection reveals the "floor" of the condition numbers at 2000 RPM is nearly twice that of those from the 1000 RPM response functions. The expectation is, then, that the force predictions from this response function will

not be as accurate as those from the 1000 RPM. Reviewing the data from Figure 44 confirms this.

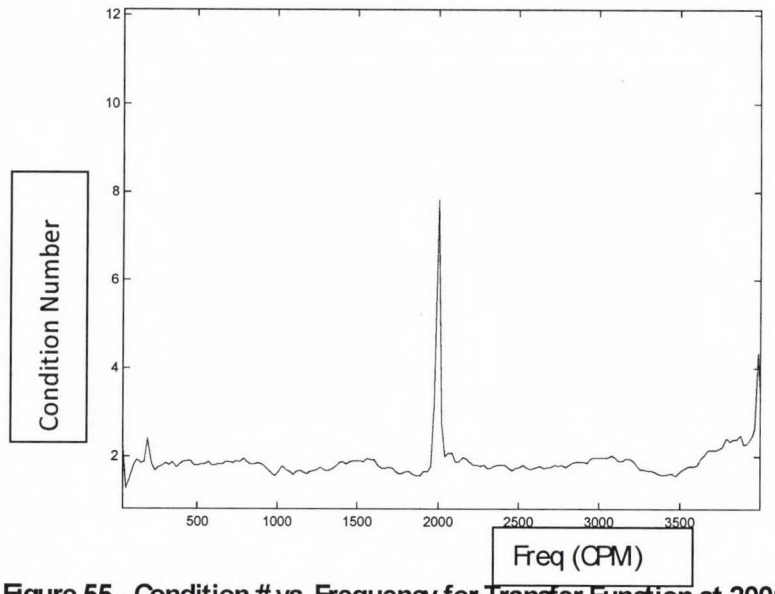

Figure 55 - Condition # vs. Frequency for Transfer Function at 2000 RPM

Figure 56 presents condition number versus frequency for the static case. Note the very high "floor" for condition number computed from the static response function. This is caused by the lack of coupling between the X and Y planes for the static case. Reviewing the very poor force calculation results for this case also confirms this correlation.

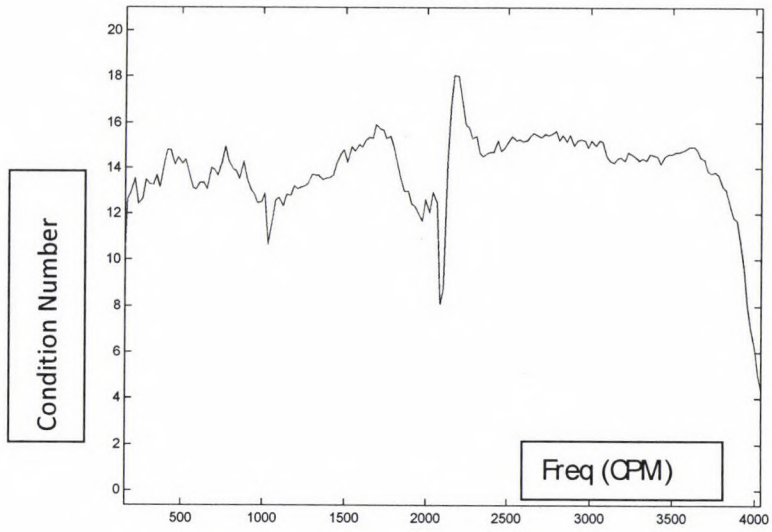

Figure 56 - Condition Number vs. Frequency for Static Transfer Function

Another factor that gives error is the departure of the unbalance speed from close proximity to the speed at which the impulse is applied. Figure 57 compares the force amplitude accuracy vs. the shaft speed at impulse used to predict the force at 1000 RPM. As the shaft speed at impulse is increased and separates from the actual forcing frequency, the prediction accuracy worsens. This makes sense since the transfer functions are dependent on the operating frequency squared. In fact, a certain amount of error should be expected as the frequency at which the impulse is applied varies from the unbalance forcing frequency in question.

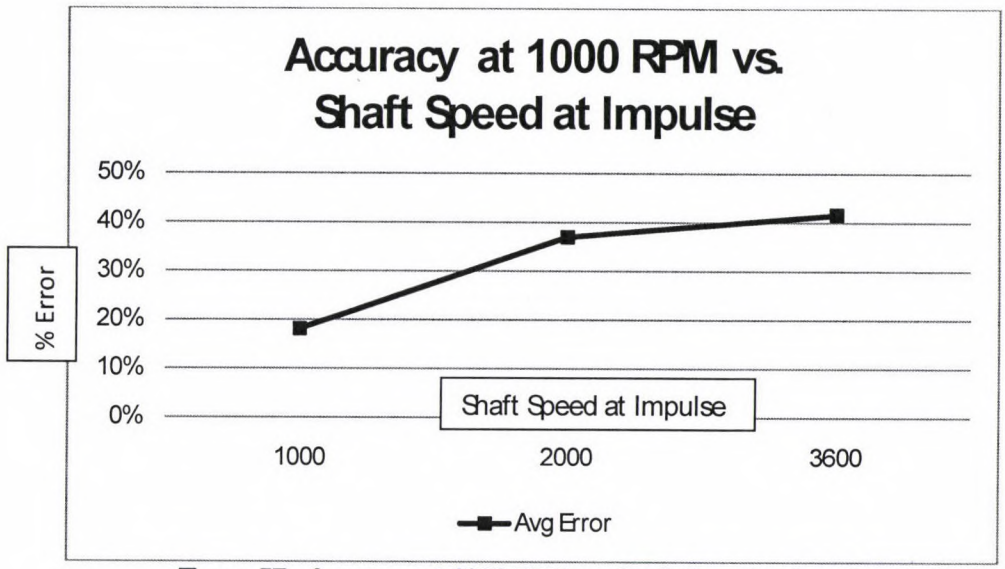

Figure 57 - Accuracy at 1000 RPM vs. Shaft Speed at Impulse

During the unbalance experiments, however, getting too close to the shaft speed at impulse can be detrimental as well. Since the condition number rises at the frequency equal to the shaft speed at which the impulse is applied, accuracy is expected to be poor near those speeds. In Figure 58, the average error is plotted against a ratio of operating speed to the speed at which the impulse is applied. The value of 1.0 on the horizontal axis indicates that the unbalance operating speed and the shaft speed at which the impulse was applied are the same. When the operating speed is 10% higher than the impulse speed, the error is minimized. Likewise it is reduced when the operating speed is 20% lower than the impulse speed. Once the frequencies continue to separate, the error rises, but seems to settle at a maximum. Note that it settles to a higher maximum above the critical speed than it does below the critical speed. As stated previously, this is likely due to the flexible rotor condition.

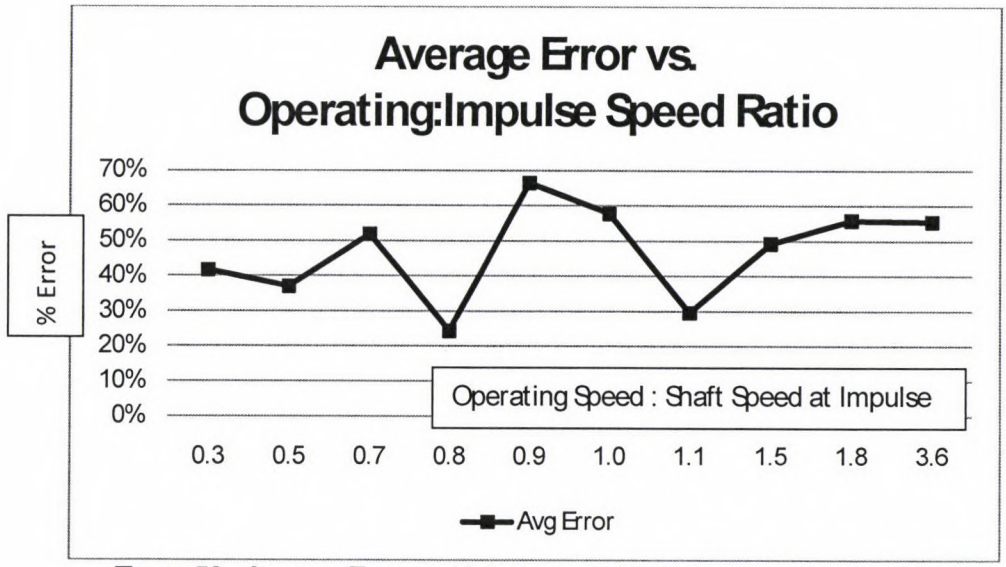

Figure 58 - Average Error vs. Unbalance to Shaft Speed at Impulse Ratio

A final discussion on error analysis involves the location of the response collected during the impulse transfer function. Most of the transfer functions used the response location at position 4 as shown in Figure 59.

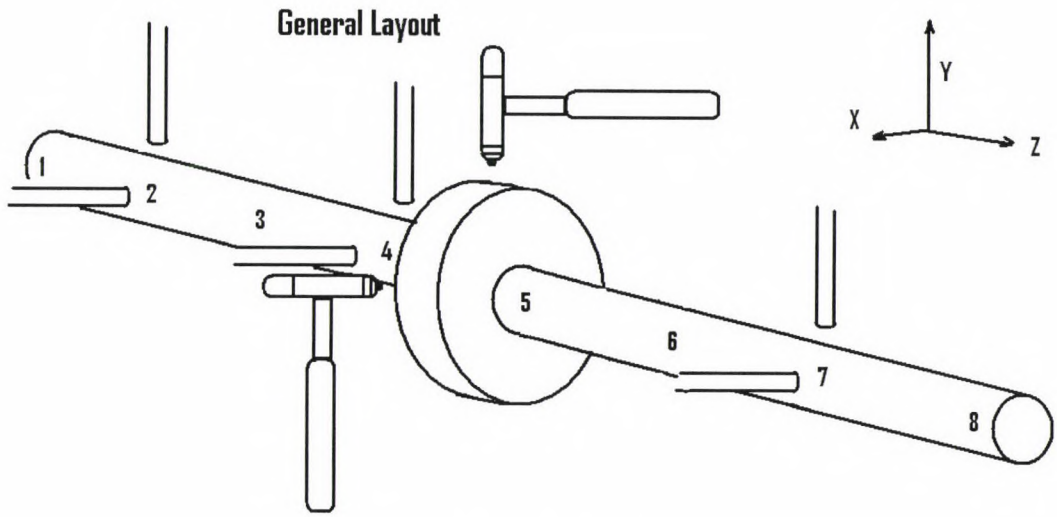

Figure 59 - (Repeat) General Layout

But, Figure 60 shows the improvement in accuracy if locations used to generate the transfer functions are chosen closer to the supporting bushings.

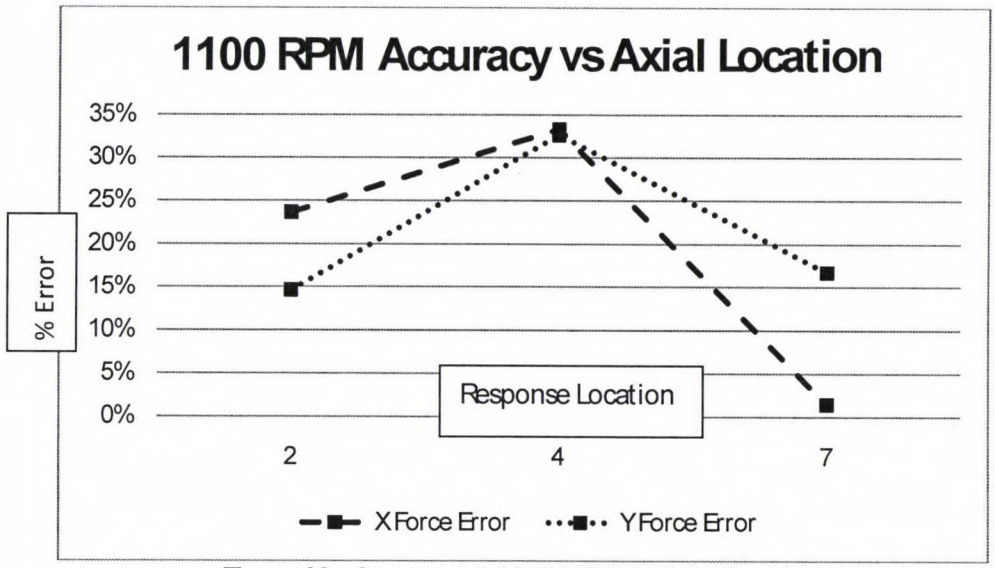

Figure 60 - Accuracy at 1100 RPM vs. Axial Location

The horizontal axis on Figure 60 lists the location identifier. Both locations 2 and 7, shown in Figure 59 produce significantly less error than the calculations at the center location 4.

Since the rotor is long and slender, and since location 4 is considered an anti-node for the first bending mode, the displacements measured there could be affected and therefore may slightly corrupt the accuracy of the force calculation. Locations 2 and 7 are much closer to the nodal points and are likely more reliable in measuring response displacements. It is suspected that a more rigid rotor, as found in real world applications, would not demonstrate the susceptibility.

Criteria for Acceptable Predictions

Before any criteria for acceptable predictions can be established, the question of what is acceptable must be addressed. Of the two parts of the force prediction solution, amplitude and frequency, the most significant is frequency. Accuracy in measured frequency is more important to industrial vibration analysis because frequency leads directly to the root source of the excessive vibration and amplitude does not. Each component in a rotating system has a unique operating frequency that is used to identify it. As mentioned previously, oftentimes aggravating conditions mask the true source of the vibration by causing the vibration response spectra to present harmonics, even when the root cause forcing function does not. By accurately predicting the forcing frequencies, and eliminating response driven harmonics, the practice of vibration analysis will be advanced significantly. In each analysis scenario studied in this dissertation, including those with high condition numbers or large deviations between desired response and impulse speeds, the forcing frequencies were predicted with errors less than 3.6%.

As shown in the error analysis section, predicting accurate amplitudes is much more challenging. The force prediction amplitude error is difficult to minimize when the rotor speed at impulse matches the desired force calculation rotor speed due to the elevated condition number. But the transfer functions are most accurate when this scenario is true. So there must be a compromise between the inaccuracy of varying the operating speed too far from the impact frequency, and moving the operating speed too close as well. With this compromise comes a necessary amount of expected error.

Fortunately, as stated previously, amplitude accuracy is not as crucial as frequency accuracy for the purposes of root cause signature analysis. Though not used to identify the root source of the vibration, it is, in many cases, used to rank the severity of the malfunction. But even when ranking severity it should be noted that amplitudes are trended parameters and a variation within that amplitude trend is more telling than the absolute amplitude accuracy.

There is more value in accurately computing load for the purpose of predicting bearing life than in aiding root cause signature analysis. The L_{10} life equation, Equation 55, predicts the expected life of 90% of a population of bearings, assuming their failure rate follows a normal distribution, given a known load and operating speed. In the past, maintenance engineers have been able to use this equation but only with the expected load, not the measured load. Typically the expected loads would include the static loads as well as the dynamic loads caused by work done by the machine. But, it is not typical to be able to include the additional load due to malfunctions. It has always been known that with additional vibration comes additional load to the bearing, but it has not been feasible to be able to compute a specific value. Given that the bearing life is more affected by load than speed, as seen in Equation 55, being able to get closer to an actual load is a very significant advancement. Since the current state of the art is to have no estimation of the malfunction force whatsoever, even moderate errors in the force prediction is a step up in technology. In Equation 55, N is the service speed, Rating is the bearing's rated radial load, and Load is the actual radial load applied.

$$L_{10} = \frac{16{,}667}{N}\left(\frac{Rating}{Load}\right)^3 \tag{55}$$

While the objective is always to minimize error, having the ability to know the amount of error is just as useful. It would be possible to calibrate the error in the procedure for a given rotor operating at a steady speed. After a precision balance was performed, a known unbalance could be added and the error calculated. For the purposes of this analysis, the amount of acceptable amplitude error will be set to less than 33%.

The criteria for acceptable predictions include considerations for condition number, response speed relative to impulse speed, response or impulse speed relative to critical speed, and axial location. Table 2 shows the specific criteria as extracted from discussions in the analysis and errors sections.

Table 2 - Criteria for Acceptable Predictions

Condition Number	All < 1.50
Operating Speed : Impulse Speed Ratio	$0.75 < r < 0.85$ or $1.05 < r < 1.2$
Operating Speed : Critical Speed Ratio, or Impulse Speed : Critical Speed Ratio	$r < 0.7$ Not recommended above 1st critical
Axial Location	As close to supporting bearing as possible

Other criteria that may or may not affect results but were assumed for this analysis include low damping and the use of eddy current probes.

Limitations

The limitations of the applications of this procedure so far include rotor and measurement setups with the following characteristics:

1) Rotors operating in rigid state, that is, less than 70% of the 1st critical speed.
2) Rotors that have the capability of variable speed control.
3) Rotors that have access to install proximity probes.
4) Rotors that have enough clearance within the shaft guarding so that an impulse could be applied while it is operating.
5) Measurement systems that use proximity probes.
6) Measurement systems that can collect at least two channels simultaneously.
7) Measurement systems with the ability to apply shaft synchronization or negative averaging.
8) Analysis systems with the ability to calculate a pseudo-inverse function.

However, it is proposed that further research be conducted to determine if case mounted accelerometers would have acceptable results as well. Lifting this limitation would be advantageous because although they are popular, proximity probes are more difficult to install than magnet mounted, case mounted accelerometers.

Conclusions

A pseudo-inverse method for force prediction in rotating industrial systems was proposed and evaluated. The limitations were delineated. It was found that the method predicts forcing frequencies well in all situations that were examined with frequency errors always less than 3.6%. The method predicts force amplitudes well in situations with rigid rotors on which impulse tests can be made at shaft speeds between 5% and 20% of the operating speed. In these situations amplitude errors are typically less than 30% which, as was discussed in the "Criteria for Acceptable Predictions" section of this dissertation, is good enough for the type of root cause analysis undertaken in most industrial applications. It was found that the technique will not predict force amplitudes well for flexible rotor situations or for scenarios when the operating impulse test can only be applied exactly at the operating speed. It is recommended that this technique be implemented as a regular part of any vibration condition monitoring and equipment troubleshooting program. As a practitioner in this field, the author plans to begin implementation of this method in order to gain further experience and insight to its applicability in the field.

Following is a review of the applications commensurate with these inverse force prediction techniques and a discussion of the original contribution to knowledge made by this research.

Application of Results

All of the education available on the subject of vibration signature analysis for the purposes of machine condition monitoring and root cause analysis centers around the characterization of vibratory forces. This is because there is no practical way to anticipate every system in which a force will be applied. Aggravating conditions such as beat frequencies, resonances, fit problems, fastener looseness, and structural weakness all significantly affect how each system responds to the same force. One system might have very high stiffness in one plane and very low stiffness in another. One system might be experiencing resonance, and another might not. If each of these systems were subjected to the same vibratory forces, each would respond very differently.

There is a disconnect between what can be taught to future vibration analysts, and what they are able to measure. Often frustration occurs because "the data just doesn't look like the book!" For example, in a vibration signature analysis class the student is taught that the force of unbalance varies with the shaft speed squared. So, if they plot the amplitude of the vibration versus the machine speed, they should be able to see that relationship in the graph. But, what if varying stiffness or even resonance occurs? In Figure 61, using the transfer function computed from the impulse applied while spinning at 1000 RPM, the predicted force is plotted along with the actual unbalance force and the vibration response versus operating speed. Since there is a critical speed on the Bently rotor at 2100 RPM, the vibration response amplifies midway through the graph. This aggravating condition hides the amplified force. The analyst has no way of knowing whether the amplified force is unbalance, a bent shaft, a shaft misalignment or any other vibratory force. This is because the amplification at resonance is so dominant.

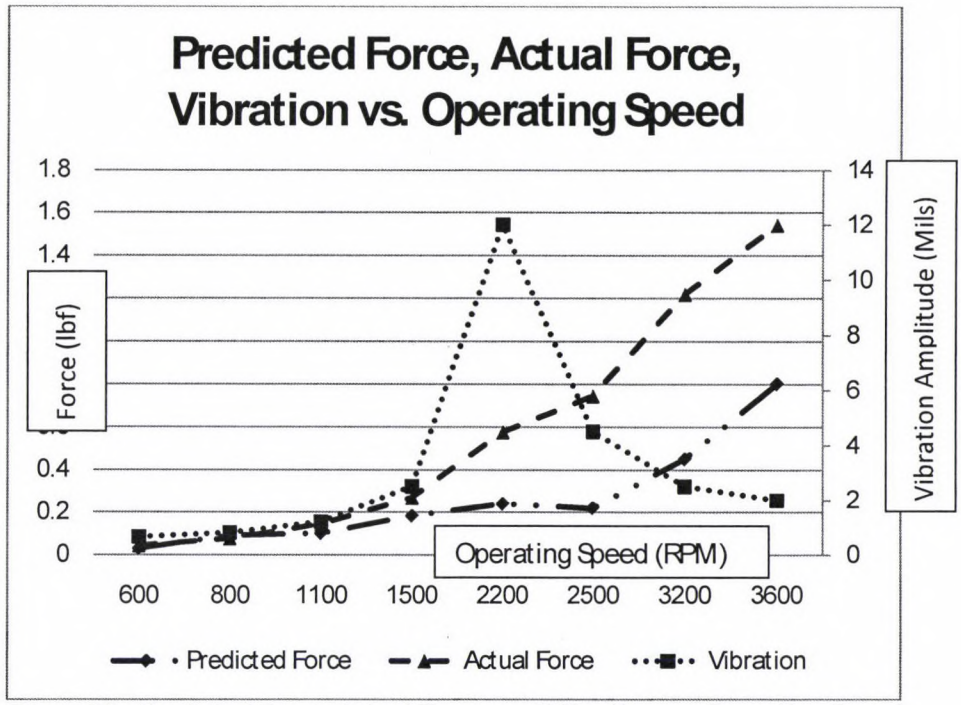

Figure 61 - Predicted Force, Actual Force, and Vibration vs. Operating Speed

But reviewing the plot of predicted force, it trends the same way that the actual unbalance forces does, as the speed increases. Even though the margin of error increases as the unbalance speed is varied away from the impulse speed, the trends still plot the same. If the analyst had both the vibration response and the predicted force plots, he would know that a resonant condition existed from the speed sensitive and massive amplitude increase. But he would also know that the amplified force is actually a simple unbalance. And, if he is able to perform a precision balance correction, then the amplification of the resonance could be mitigated. Without this information, the analyst could only guess at which force to consider.

In addition, if the analyst only had vibration data but suspected unbalance, she would have to perform a balance correction procedure using trial weights in order to quantify the amount of unbalance. However, if she is able to know the force with some degree of accuracy even if only

within 30%, then the actual amount of unbalance weight could be estimated before a procedure was even started.

In addition to improving the ability to diagnose vibratory forces, force prediction using pseudo-inverse techniques can help to prioritize the order in which repairs are made. For example, suppose that a unit of unbalance force is applied to a rotor mounted on springs for isolation purposes. Then assume double the amount of unbalance is applied to a rotor installed with an inertia base that is heavily anchored and grouted. It is conceivable that the response within the isolated machine would increase vibration levels several orders of magnitude more than the effect that double the unbalance would have when applied to the second rotor.

If an analyst were trying to determine which machine to repair, he might choose the first machine simply because the vibration amplitudes are so much higher than the second. But considering that the force is higher on the second, and the fact that the relative vibration between the bearings and the shaft are even greater on the inertia base machine than the isolated machine, the analyst would be making the wrong choice for priority. Shaft vibration relative to bearing vibration is low on isolated machines since both components move together and in-phase. The ability to quantify the unbalance force, as provided by the pseudo-inverse method for force prediction, would prevent this mistake.

Lastly, with the technology available today, an analyst who wished to simulate loadings using finite elements on a rotor would have to do so without the ability to quantify vibratory forces. She would not be able to include actual forces applied. She would be limited to theoretical

forces which likely do not include malfunction forces. With force prediction, her results could be much more realistic.

Original Contribution to Knowledge

The objective of this research has been to advance the state-of-the-art-and-practice in industrial vibration signature applications to add the capability to determine forcing functions based upon vibration measurements made on installed and operating rotating industrial machines. Specifically, the goal was to compute the force of unbalance as a function of frequency and time on rotating industrial equipment. This computation would include accurate frequency, amplitude, and direction. Having this information available will allow the analyst to interpret already characterized forcing function data rather than the unpredictable response function information. Prior to the current research there has been no capability to compute forcing functions within rotating equipment using inverse methods on vibration response data.

Load quantification, although common in the aerospace and automotive industries, is not common in the industrial maintenance community. The forward methods are too cumbersome to use in such an environment. Inverse methods, using technologies that are common to industrial maintenance, will open a door to predicting actual loads. Bearings that spall prematurely, shafts that repeatedly crack, and couplings that deform could be analyzed using the predicted loads. Designers might find more loads than expected due to installation and use errors.

A number of authors have established the rules for which force prediction works on a structural vibration system. Before the work reported here, no such rules existed for a rotating shaft application. Determining the criteria for which this type of force prediction can be made accurately will ensure the success of the procedure. Success with these methods will lead to more applications attempted, and more criteria established, thereby improving the technology.

Recommendations for Future Research

Further research is needed to improve the synchronizing techniques used to "clean" the complete response so that more accurate force amplitude can be predicted with impulses applied exactly at normal operating speed.

Further studies are also needed to determine if case mounted accelerometers will give similar or better results. Lifting this limitation would be advantageous because although they are popular, proximity probes are more difficult to install than magnetically held, case mounted accelerometers.

Another option for further research involves a source of error mentioned in the "Background" section of this dissertation. It is the possibility of skidding of the modal hammer tip while it is in contact with the rotating shaft. One way to determine the amount of this error is to vary the tip hardness by changing tips. All modal hammers use tips of different materials in order to vary the duration of the applied impulse. By varying the duration of the applied impulse, the frequency response range is changed. Installing a harder tip (e.g. bronze) shortens the duration of the impulse and increases the frequency response range. Installing a softer tip (e.g. rubber)

lengthens the duration of the impulse and decreases the frequency response range. In general, best practices for the application of a modal hammer suggest selecting a tip that produces a frequency response range slightly above the range under consideration. For the purposes of testing this source of error, the hammer tip should be varied for the same system and same conditions. Then the amount of error could be computed as a function of hammer tip used.

More research could also be done to determine if force amplitude accuracy can be improved by using more than two perpendicular response measurements at any one location. It was suggested in this dissertation that more responses measured circumferentially around the periphery of the shaft would not likely improve the results, but it may be worth researching to be sure. Like previous research on the uni-axial structural systems (Fabunmi, 1986), more responses could be measured and added to the transfer function matrix. If this were the case more responses will be measured than forces desired making the transfer function matrix rectangular, and over-determined. A matrix that is over-determined will be rank deficient which requires the same alternate inverse technique, as was used in this study as a result of ill-conditioning, in order to invert the matrix.

Additional research is needed to determine the criteria for the speed at which the force of unbalance is so low that the force prediction is unreliable.

Lastly, more research is needed to determine the accuracy of forces applied at frequencies different from the operating speed.

Acknowledgements

The author of this dissertation would like to acknowledge the Department of Mechanical Engineering at Colorado State University, Bently-Nevada Corporation, Fred W. Smith and the rest of the academic committee, Donald and Patricia Stansloski, and Leslie Arnold.

The Department of Mechanical Engineering at Colorado State University made the Dynamics Lab and the Bently-Nevada equipment readily available. Bently-Nevada Corporation donated the rotor kit, the proximity probes, and the probe signal conditioners.

Fred W. Smith was the academic advisor for this dissertation and provided immediate and insightful responses to the technical challenges herein. The remaining members of the academic committee, Bryan Willson, Paul Wilbur, and Bogusz Bienkiewicz provided excellent feedback during the preliminary and final defenses.

This dissertation would not likely have been completed without the tremendous encouragement and support provided by the author's wife, Leslie Arnold, and parents, Donald and Patricia Stansloski.

Glossary

Aggravating Conditions – circumstances that arise in industrial systems that alter the response to an input force

Accelerometer – vibration transducer that measure acceleration as its native unit

Condition Number – measure of a mathematical problem's amenability to numerical calculations, problems with low condition numbers are said to be well condition, problems with high condition numbers are said to be ill conditioned

Coupler – device that connects two co-linear shafts together

Critical Speed – shaft speed at which resonance occurs. *See also resonance*

Flexible Rotor – shaft that operates above 70% of its first critical speed. *See also critical speed*

Frequency Bin – range of frequency within a digital spectrum, dependant on sampling rate and the number of samples collected

Harmonic – integer multiple of a fundamental frequency

Ill Conditioned – numerical problem in which small error in initial data can lead to large errors in the solution, associated with a large condition number. *See also Condition Number.*

Impulse Function – a brief input force signal typically applied to a system using a modal hammer. *See also Modal Hammer*

Impulse Speed – shaft operating speed at the time an impulse function was applied

Modal Hammer – hammer fitted with a dynamic force transducer and interchangeable tips (which determine the frequency range over which the impulse function is effective) and is used to apply impulse function

Modal Superposition – a method used to compute a system's response whereby factored mode shapes are summed

2-Norm – also known as the Euclidean Norm, gives an calculation of the size of a vector by computing its Euclidean distance

Negative Averaging – process in vibration signal processing that collects a first sample of data, and then subtracts all subsequent samples from the first

Operating Speed – speed at which an unbalance weight is applied to the disk for the purpose of computing its force

Operating Speed : Impulse Speed Ratio - ratio of the rotor speed to the speed at which the rotor was turning when the impulse function was applied

Portable Shaker – device that uses an input signal in order to drive a corresponding vibration output, vibration is typically transmitted using a long slender rod called a stinger. *See also Stinger*

Principal Frequency – a natural frequency of a vibrating system, a function of mass, stiffness, and damping

Proximity Probe – vibration sensor that utilizes an eddy current field to measure displacement

Pseudo-inverse – generalized inverse used in place of a traditional inverse when it is not invertibleor difficult to invert. The most common is the Moore-Penrose pseudo-inverse which is used to compute a best fit, or least squares solution to a set of linear equations that lacks a unique solution, can also be computed using singular value decomposition

Random Frequency Generator – device that synthesizes a vibration signal with non-periodic frequencies

Rank – maximum number of independent rows or columns in a matrix

Resonance – condition that occurs in a vibrating system when a natural frequency equals a forcing frequency

Rigid Rotor – shaft that operates below 70% of its first critical speed

Rotor – rotating component, usually a shaft

Singular Matrix – square matrix that is not invertible

Singular Value Decomposition (SVD) – factorization of a rectangular matrix, if a SVD is $M=U\Sigma V^*$, then the diagonals of Σ are the singular values of M, and the columns of U and V^* are the left and right singular vectors for the corresponding values

Skew Symmetric Matrix – square matrix whose transpose is also its negative

Spectral Resolution – or bin width, is a measure of the available accuracy with respect to frequency within a digital vibration spectrum, is a function of sampling rate and the number of samples

Stinger – long slender rod used to transmit vibration from a portable shaker to a system. *See also Portable Shaker*

Synchronized Frequencies – identical vibration frequencies whose timing is adjusted so that they are in-phase

Transfer Function – a function in the frequency domain that defines how a system's output relates to its input, in vibration systems a common transfer function is called the frequency response function

Variable Frequency Generator – device that synthesizes a vibration signal with adjustable frequency output

Vibration Signature Analysis – process whereby vibration spectra are analyzed in order to determine the source of equipment malfunctions

Bibliography

Avitabile, P., & Piergentili, F. (1999). Generation of Input Forcing Functions Through the Use of Measured Response and the FRF's. *Proceedings of the 17th International Modal Analysis Conference. February.* Orlando, FL: IMAC.

Bartlett, F. D., & Flannelly, W. G. (1979). Model Verification of Force Determination for Measuring Vibratory Loads. *Journal of the American Helicopter Society , 24*, 10-18.

Bendat, J. S., & Piersol, A. G. (1993). *Engineering Applications of Correlation and Spectral Analysis.* New York: John Wiley & Sons.

Chiementin, X., Bolaers, F., Rasolofondraibe, L., & Dron, J. P. (2008). Localization and Quantificationof Vibratory Sources: Application to Predictive Maintenance of Rolling Bearings. *Journal of Sound and Vibration* , 331-347.

Desanghere, G., & Snoeys, R. (1985). Indirect Identification of Excitation Forces by Modal Coordinate Transformation. *Proceedings of the 3rd International Modal Analysis Conference. 1*, pp. 685-690. Orlando, FL: IMAC.

Dos Santos, M. A., & Varoto, P. S. (1998). Indentification of Dynamic Loads: A Comparative Analysis Between Time and Frequency Domain Response Techniques.

Ehrich, F. F. (1992). *Handbook of Rotordynamics.* New York: McGraw-Hill, Inc.

Ewins, D. (2000). *Modal Testing: Theory and Practice, 2nd. Edition.* London, UK: Research Studies Press.

Fabunmi, J. (1986). Effects of Structural Modes on Vibratory Force Determination by the Pseudoinverse Technique. *AIAA Journal , 24* (3), 504-509.

Hillary, B., & Ewins, D. J. (1984). The Use of Strain Gages in Force Determination and Frequency Response Measurements. *Proceedings of the 2nd International Modal Analysis Conference. 1*, pp. 627-634. Orlando, FL: IMAC.

Matsumura, S. (1985). Application of Force Identification Techniques to Automobile Engines. *Proceedings of the 10th International Seminar on Modal Analysis. September.* K.U. Leuven, Belgium: IMAC.

Okubo, N., Shimamura, S., & Toi, T. (2006). Identification of Excitation Force Generated From Automobile Engine in High Frequency Range. *International Conference on Noise and Vibration Engineering* (pp. 3985-3991). Louvain, Belgium: Proceeedings of ISMA2006: International Conference on Noise and Vibration Engineering.

Okubo, N., Tanabe, S., & Tatsuno, T. (1985). Identification of Forces Generated by a Machine Under Operating Conditions. *Proceedings of the 3rd International Modal Analysis Conference* (pp. 920-927). Orlando, FL: IMAC.

Peters, D., Nordmann, R., Domes, B., & Maass, P. (2004). Inverse Determination of Imbalance Distributions. *Eighth International Conference on Vibrations in Rotating Machinery* (pp. 521-530). Swansea, United Kingdom: Professional Engineering Publishing.

Rao, S. S. (1986). *Mechanical Vibrations.* Reading, Massachusetts: Addison-Wesley Publishing Company.

Stevens, K. (1987). Force Indentification Problems - An Overview. *Proceedings of the 1987 SEM Spring Conference on Experimental Mechanics. June*, pp. 838-844. Houston, TX: SEM.
Strang, G. (1988). *Linear Algebra and Its Applications, 3rd Edition.* Fort Worth, Texas: Harcourt Brace Jovanovich College Publishers.
Toi, T., Aoyama, K., & Okubo, N. (1995). Prediction of Transmitted Force Between Components Under Operating Condition for Reduction of Vibration and Noise. *Journal of the Japan Society for Precision Engineering* , 213-217.
Varoto, P. (1996). *The Rules for the Exchange and Analysis of Dynamic Information in Structural Vibration, Ph.D. Dissertation.* USA: Iowa State University.
Yuan, C.-H., Zhu, X.-M., Zhang, G.-L., & Zhang, W.-H. (2007). Indirect Engineering Estimation of Force Excited by Machinery Vibration Sources of Ship. *Journal of Ship Mechanics* , 961-973.
Zutavern, Z. S., & Childs, D. W. (2008). Identification of Rotordynamic Forces in a Flexible Rotor System Using Magnetic Bearings. *Journal of Engineering for Gas Turbines and Power , 130* (2).

Appendix A – Matlab Program Written to Compute Closed Form Solution Results

```
%
%  This program will models a simple spinning rigid shaft and disk.
%  The shaft is pinned at one end, and the opposite end has a flexible
bearing supporting
%  the disk.
%  The equations of motion have been created, and the response function
entered here in terms
%  of running speed (omega), lateral moment of inertia (I0), polar
moment of inertia J,
%  length of the shaft (length), horizontal and vertical bearing
stiffness (kx and ky), and vibration
%  frequency (w).
%
%  Author:  Mitchell Stansloski, PE
%  Date:    March 9, 2002
%
%  This program is designed specifically for the Bently Rotor Kit.
%
%  An unbalance force is applied in two directions, and a response is
calculated.
%  Then the calculated responses are premulitplied by the pseudoinverse
of the response function.
%  New forces are then calculated and compared to the original.
%
%  Assign metric values to variables
%
m=0;
J = 6.452E-4;
I0 = 8.39E-3;
length = 0.09525;
kx = 350000;
ky = 350000;
omega = 188*1.1;
w = (1:1000);
%bx = kx*length^2;
%by = ky*length^2;
%c = I0;
%d = kx*ky*length^2;
%e = I0*(kx+ky)+(J*omega/length)^2;
%g = (I0/length)^2;
%h = omega*J;
%
%  Compute the pricipal frequencies
```

```
w1 = (((J^2*omega^2/length^2+(kx+ky)*I0)-
(((J*omega/length)^2+(kx+ky)*I0)^2-
4*I0^2*kx*ky)^(1/2))/(2*I0^2/length^2))^(1/2);
w2 =
(((J^2*omega^2/length^2+(kx+ky)*I0)+(((J*omega/length)^2+(kx+ky)*I0)^2-
4*I0^2*kx*ky)^(1/2))/(2*I0^2/length^2))^(1/2);
%
%  Compute the transfer functions
for m = 1:1000
   axy(m) = (w(m) * .1213i) / (1111388906-
5874.625*w(m)^2+.007758*w(m)^4);
   ayx(m) = -(w(m) * .1213i) / (1111388906-
5874.625*w(m)^2+.007758*w(m)^4);
   axx(m) = (3175 - 8.39E-3 * w(m)^2) / (1111388906-
5874.625*w(m)^2+.007758*w(m)^4);
   ayy(m) = (3175 - 8.39E-3 * w(m)^2) / (1111388906-
5874.625*w(m)^2+.007758*w(m)^4);
end
%
%  Compute the original forces
%
for n=1:1000
   if n==omega
   fy(n)=10i;
   fx(n)=10;
else
   fy(n)=0;
   fx(n)=0;
end
end
%
%  Compute the response to those unbalance forces
%
for m=1:1000
a(1,1)=axx(m);
a(1,2)=axy(m);
a(2,1)=ayx(m);
a(2,2)=ayy(m);
f(1,1)=fx(m);
f(2,1)=fy(m);
r=a*f;
x(m)=r(1,1);
y(m)=r(2,1);
end
%
%  Compute the new forces by premultiplying the transfer function
for m=1:1000
a(1,1)=axx(m);
a(1,2)=axy(m);
a(2,1)=ayx(m);
a(2,2)=axx(m);
r(1,1)=x(m);
r(2,1)=y(m);
%  Compute the conditon number of the response matrix
condition(m) = cond(a);
newf=(pinv(a))*r;
```

```
newfx(m)=newf(1,1);
newfy(m)=newf(2,1);
end
%
%  Plot the results
plot(w,real(axx),w,imag(axx))
xlabel('Frequency (Rad/Sec)')
ylabel('Amplitude (in)')
title('Axx (Ayy) Response Spectrum','FontSize',12)
pause
plot(w,real(ayy),w,imag(ayy))
xlabel('Frequency (Rad/Sec)')
ylabel('Amplitude (in)')
title('Ayy Response Spectrum','FontSize',12)
pause
plot(w,real(axy),w,imag(axy))
xlabel('Frequency (Rad/Sec)')
ylabel('Amplitude (in)')
title('Axy Response Spectrum','FontSize',12)
pause
plot(w,real(ayx),w,imag(ayx))
xlabel('Frequency (Rad/Sec)')
ylabel('Amplitude (in)')
title('Ayx Response Spectrum','FontSize',12)
pause
plot(w,fx)
xlabel('Frequency (Rad/Sec)')
ylabel('Amplitude (N)')
title('X-Dir Force','FontSize',12)
pause
plot(w,imag(fy))
xlabel('Frequency (Rad/Sec)')
ylabel('Amplitude (N)')
title('Y-Dir Force','FontSize',12)
pause
plot(w,real(x))
xlabel('Frequency (Rad/Sec)')
ylabel('Amplitude (in)')
title('X Response Spectrum','FontSize',12)
pause
plot(w,imag(y))
xlabel('Frequency (Rad/Sec)')
ylabel('Amplitude (in)')
title('Y Response Spectrum','FontSize',12)
pause
plot(w,real(newfx))
xlabel('Frequency (Rad/Sec)')
ylabel('Amplitude (N)')
title('Calculated Fx','FontSize',12)
pause
plot(w,imag(newfy))
xlabel('Frequency (Rad/sec)')
ylabel('Amplitude (N)')
title('Calculated Fy','FontSize',12)
pause
plot(w,condition)
xlabel('Frequency (Rad/sec)')
```

```
ylabel('Condition')
title('Response Matrix Condition Number','FontSize',12)
```

Appendix B – Matlab Program to Compute Transfer Functions

```
% Input the data
%fs=input('Enter the sampling frequency ');
%N=input('Enter the number of samples ');
%avg=input('Enter the number of averages ');
%sens=input('Enter transducer sensitivity');
%Amp=1/sens;
fs=12000;
N=4*8192;
sens=.2;
Amp=1/sens;
%
%  Generate a frequency array
bin_num = 1:N;
t = (bin_num-1)/fs;
bin_size = fs/N;
f(N/2+1)=fs/2;
f(1:N/2+1) = (bin_num(1:N/2+1)-1).*bin_size;
f(N/2+2:N) = f(N/2:-1:2);
%
%  Convert frequency to rad/sec and CPM
w = f*2*pi;
CPM = f*60;
%
%  Set channels from input matrix
%
a4=-Amp*a(4,1:N);
a5=(1/.01)*a(5,1:N);
%
% Re-center the prox probe data around zero
%
a4=detrend(a4);
%a5=detrend(a5);
%
%
%  compute normalized fft's for all channels
A4=fft(a4)/(N/2);
A5=fft(a5)/(N/2);
%
plot(CPM(1:N/2),abs(A4(1:N/2)))
pause
plot(CPM(1:N/2),abs(A5(1:N/2)))
pause
%
%  Compute the FRF
Hyy=A4./A5;
%  Plot the FRF
```

```
plot(CPM(1:N/2),real(Hyy(1:N/2)),CPM(1:N/2),imag(Hyy(1:N/2)))
pause
save Hyy Hyy
```

Appendix C– Matlab Program Used to Compute Predicted Forces

```
%  This program will calculate forces by using a measured vibration
response and
%  the Frequency Response Function.  All calculations are done with the
%  data in the frequency domain
%
%  Author:  Mitchell Stansloski, PE
%  Date:    Sept 13, 2009
%
%  This program is designed specifically for data collected with
proximity probes.
%
%  A 2x2 FRF matrix is inverted and pre-multiplied by a 2x1 response
%  matrix in order to extract 2 force functions.
%
%
%  Assign values to variables
%
fs=12000;
N=4*8192;
sens=.2;
Amp=1/sens;
load Hxx
load Hyy
load Hxy
load Hyx
%
%  Generate a frequency array
bin_num = 1:N;
t = (bin_num-1)/fs;
bin_size = fs/N;
f(N/2+1)=fs/2;
f(1:N/2+1) = (bin_num(1:N/2+1)-1).*bin_size;
f(N/2+2:N) = f(N/2:-1:2);
%
%  Convert frequency to rad/sec and CPM
w = f*2*pi;
CPM = f*60;
%
%  Set channels from response matrix
%
a4x=Amp*x(7,1:N);
a4y=Amp*y(7,1:N);
%
% Re-center the prox probe data around zero
%
a4x=detrend(a4x);
```

```
a4y=detrend(a4y);
%
%  compute normalized fft's for all channels
%
A4X=fft(a4x)/(N/2);
A4Y=fft(a4y)/(N/2);
%
%  Plot FFT's for Data Verification
%
plot(CPM(1:N/2),abs(A4X(1:N/2)))
pause
plot(CPM(1:N/2),abs(A4Y(1:N/2)))
pause
%
%  Build the Transfer Function and Response Matrices
%  Iterate through each sample
%
for i = 1:N
   %  Build the FRF Matrix
   H(1,1) = Hxx(i);
   H(1,2) = Hxy(i);
   H(2,1) = Hyx(i);
   H(2,2) = Hyy(i);
   %  Check the Condition of the FRF
   condition(i)=cond(H);
   %  Build the response matrix (4x1)
   Y(1,1) = A4X(i);
   Y(2,1) = A4Y(i);
   %  Calculate the force matrix using the pseudoinverse function
   X = (pinv(H))*Y;
   NewX(i)=X(1,1);
   NewY(i)=X(2,1);
   %
   %  Calculate the force using the Hermetian (transpose of the complex
conjugate)
   %  X = (inv(H'*H)*H')*Y;
   %  Extract the individual forces from the force matrix for each
sample
   %  X1(i) = X(1,1);
end
%
%  Plot the condition number of the transfer function
plot(CPM(1:N/2),condition(1:N/2))
pause
%
%  Plot the forcing function
%
plot(CPM(1:N/2),abs(NewX(1:N/2)))
pause
plot(CPM(1:N/2),abs(NewY(1:N/2)))
pause
```

Appendix D – Matlab Program Used to Compute Standard Deviation and Coherence

```
%  This Matlab program was written by Mitchell Stansloski on March 12,
2010
%  and is used to compute standard deviation in the transfer function
data
%  as well as coherence between the hammer strike inputs and vibration
displacement
%  outputs.
%
%Input the data
load A1
load A2
load A3
load A4
load A5
load A6
load OP
%
%  Set the variables
a1=A1;
a2=A2;
a3=A3;
a4=A4;
a5=A5;
a6=A6;
a7=OP;
fs=12000;
N=4*8192;
sens=.2;
Amp=1/sens;
%
%  Generate a frequency array
bin_num = 1:N;
t = (bin_num-1)/fs;
bin_size = fs/N;
f(N/2+1)=fs/2;
f(1:N/2+1) = (bin_num(1:N/2+1)-1).*bin_size;
f(N/2+2:N) = f(N/2:-1:2);
%
%  Convert frequency to rad/sec and CPM
w = f*2*pi;
CPM = f*60;
%
%  Set channels from input matrices
%
a14=Amp*a1(4,1:N);
a15=(1/.01)*a1(5,1:N);
```

```
%
a24=Amp*a2(4,1:N);
a25=(1/.01)*a2(5,1:N);
%
a34=Amp*a3(4,1:N);
a35=(1/.01)*a3(5,1:N);
%
a44=Amp*a4(4,1:N);
a45=(1/.01)*a4(5,1:N);
%
a54=Amp*a5(4,1:N);
a55=(1/.01)*a5(5,1:N);
%
a64=Amp*a6(4,1:N);
a65=(1/.01)*a6(5,1:N);
%
a74=Amp*a7(4,1:N);
a75=(1/.01)*a7(5,1:N);
%
%
% Re-center the prox probe data around zero
%
a14=detrend(a14);
a24=detrend(a24);
a34=detrend(a34);
a44=detrend(a44);
a54=detrend(a54);
a64=detrend(a64);
a74=detrend(a74);
%
%
%  compute normalized fft's for all channels
%
A14=fft(a14)/(N/2);
A15=fft(a15)/(N/2);
A24=fft(a24)/(N/2);
A25=fft(a25)/(N/2);
A34=fft(a34)/(N/2);
A35=fft(a35)/(N/2);
A44=fft(a44)/(N/2);
A45=fft(a45)/(N/2);
A54=fft(a54)/(N/2);
A55=fft(a55)/(N/2);
A64=fft(a64)/(N/2);
A65=fft(a65)/(N/2);
A74=fft(a74)/(N/2);
A75=fft(a75)/(N/2);
%
%
% Compute FRF's
```

```
%
H1=A14./A15;
H2=A24./A25;
H3=A34./A35;
H4=A44./A45;
H5=A54./A55;
H6=A64./A65;
%
%  Coupute the power spectra for the transfer functions
%
PH1=(H1.*conj(H1)).^.5;
PH2=(H2.*conj(H2)).^.5;
PH3=(H3.*conj(H3)).^.5;
PH4=(H4.*conj(H4)).^.5;
PH5=(H5.*conj(H5)).^.5;
PH6=(H6.*conj(H6)).^.5;
%
% Average the Transfer Functions
%
Havg=((PH1)+(PH2)+(PH3)+(PH4)+(PH5)+(PH6))/6;
%
%
% Compute Standard Deviation of the Transfer Functions
%
for k=1:16384
   x=[PH1(k) PH2(k) PH3(k) PH4(k) PH5(k) PH6(k)];
   s(k)=std(x);
   error(k)=(s(k)/Havg(k)*100);
end
%
%  Plot the data
%
plot(CPM(1:N/2),abs(Havg(1:N/2)),CPM(1:N/2),PH1(1:N/2),CPM(1:N/2),PH2(1
:N/2),CPM(1:N/2),PH3(1:N/2),CPM(1:N/2),PH4(1:N/2),CPM(1:N/2),PH5(1:N/2)
,CPM(1:N/2),PH6(1:N/2))
title('Transfer Function Repeatability')
xlabel('Frequency (CPM)')
ylabel('Amplitude (g/lbf)')
pause
plot(CPM(1:N/2),s)
pause
plot(CPM(1:N/2),error)
title('Transfer Function Standard Deviation')
xlabel('Frequency (CPM)')
ylabel('Deviation as Percent of Average')
pause
%
%  Compute Coherence
%
PA14=A14.*conj(A14);
```

```
PA15=A15.*conj(A15);
PA24=A24.*conj(A24);
PA25=A25.*conj(A25);
PA34=A34.*conj(A34);
PA35=A35.*conj(A35);
PA44=A44.*conj(A44);
PA45=A45.*conj(A45);
PA54=A54.*conj(A54);
PA55=A55.*conj(A55);
PA64=A64.*conj(A64);
PA65=A65.*conj(A65);
PA74=A74.*conj(A74);
sumP4=PA14+PA24+PA34+PA44+PA54+PA64;
sumP5=PA15+PA25+PA35+PA45+PA55+PA65;
sum54=conj(A15).*A14+conj(A25).*A24+conj(A35).*A34+conj(A45).*A44+conj(
A55).*A54+conj(A65).*A64;
sum45=conj(A14).*A15+conj(A24).*A25+conj(A34).*A35+conj(A44).*A45+conj(
A54).*A55+conj(A64).*A65;
H1=sum45./sumP4;
H2=sumP5./sum54;
coh=real(H1./H2);
%
%  Plot coherence
%
plot(CPM(1:N/2),coh(1:N/2))
title('Coherence vs Frequency')
xlabel('Frequency (CPM)')
ylabel('Coherence (dimensionless)')
pause
%
```